Gas exchange model using heterogeneous diffusivity to study internal browning in 'Conference' pear

Bayu Nugraha[1,3], Pieter Verboven[1,*], Bert E. Verlinden[2], Celine Verreydt[1], Matthieu Boone[4,5], Iván Josipovic[4], Bart M. Nicolaï[1,2]

[1]BIOSYST-MeBioS, KU Leuven, Willem de Croylaan 42, 3001 Leuven, Belgium

[2]Flanders Centre of Postharvest Technology, Willem de Croylaan 42, 3001 Leuven, Belgium

[3]Department of Agricultural and Biosystems Engineering, Universitas Gadjah Mada, Jl. Flora No. 1, Sleman, Yogyakarta 55281, Indonesia

[4]Centre for X-ray Tomography – UGCT, Ghent University, Proeftuinstraat 86/N3, 9000 Gent, Belgium

[5]Radiation Physics, Dept. Physics and Astronomy, Ghent University, Proeftuinstraat 86/N12, 9000 Gent, Belgium

Corresponding author: Pieter Verboven at BIOSYST-MeBioS, KU Leuven,
Willem de Croylaan 42, 3001 Leuven, Belgium
Tel.: +32 16 32 14 53; fax.: +32 16 3 22955
e-mail: pieter.verboven@kuleuven.be

Keywords **:** respiration, controlled atmosphere storage, hypoxia, X-ray CT, oxygen, carbon dioxide, respiratory quotient

Highlights:

- Pear tissue microstructure was imaged using X-ray CT
- Heterogeneous gas diffusivity maps were derived from spatial porosity profiles
- Internal gas concentrations in pear were computed using heterogeneous diffusivity
- Pear tissue subject to energy deficiency corresponded to actual browning patches

Abstract

Internal gas gradients in pear fruit during controlled atmosphere storage depend on the effective gas diffusivity of the tissue. The diffusivity varies over the fruit organ due to the heterogeneous tissue microstructure across the fruit. This study implemented effective diffusivity maps reflecting the heterogeneous structure to predict internal gas gradients and relate the result to the occurrence of internal browning. Diffusivity maps of different pears were calculated from X-ray CT based porosity maps. Internal oxygen (O_2), carbon dioxide (CO_2) and respiratory quotient (RQ) levels were computed using a reaction-diffusion model incorporating the heterogeneous effective diffusivity map. Critical O_2 and RQ levels for the shift from respiration to fermentation were defined based on the respiratory-fermentative energy balance of the cells. The model was indirectly validated by comparing RQ level contours with nondestructive 3D images of the internal browning of the pears after storage at 1.0 kPa and 0.5 kPa O_2, combined with 0.7 kPa CO_2 at 1°C. The distribution of the internal gas concentrations and RQ was affected by the heterogeneity of the diffusivity. The results also confirmed the incidence of internal browning when the O_2 and RQ were under or above critical O_2 and RQ limits, respectively. The fermentation process was indicated to be dominant when the tissue's RQ^* went above 2.12 (or at 0.044 kPa O_2). The tissue volumes where O_2 and RQ levels were critical corresponded reasonably well to browning-affected tissues of pears with different shapes. The pear with more shallow gas gradients showed less symptoms of browning.

1 Introduction

After harvest, 'Conference' pears (*Pyrus Communis* L. cv. 'Conference') are typically stored under controlled atmosphere (CA) storage to decrease the respiration rate and thus prolong storage life (Brady and Romani, 1988). In CA storage decreased levels of O_2 and increased levels of CO_2 are combined with a low temperature.

The skin and different tissues inside the fruit present a resistance to gas transport and are thus responsible for gas gradients inside the fruit (Rajapakse et al., 1990; Perez and Beaudry, 1998; Zhang and Bunn, 2000; Lammertyn et al., 2003b; Ho et al., 2011, 2013, 2016). The O_2 partial pressure generally declines while the CO_2 partial pressure increases from the skin to the fruit center (Lammertyn et al., 2003b; Ho et al., 2016). At very low O_2 partial pressure in the storage atmosphere, the diffusion resistance increases the possibility of hypoxic or even anoxic conditions inside the stored fruit which gradually shifts the central metabolism to a fermentation dominated process. Although typical plant cells may temporarily survive the low oxygen stress (Drew, 1997; Toro and Pinto, 2015), they would eventually lose cell membrane integrity due to insufficient energy supply by fermentation only (Rawyler et al., 1999; Franck et al., 2007). Such a condition has been suggested to lead to symptoms of internal browning and cavity formation in pear tissue (Lammertyn et al., 2003c,d; Saquet et al., 2003; Franck et al., 2007). The extent and spatial distribution of the disorder has been hypothesized to be related to the gas concentration contours inside the fruit (Lammertyn et al., 2003b).

To avoid fermentation and internal browning, the O_2 partial pressure in regular CA is set at a safe level well above the critical O_2 level or anaerobic compensation point (ACP). Dynamic CA (DCA) storage allows the modified gas levels to be closer to the ACP as it is naturally controlled by a biological signal of the fruit indicating that fermentation becomes important. Different methods can be used to implement DCA; the main available technologies include the measurement of a chlorophyll fluorescence (CF) response (Prange et al., 2002; Mditshwa et al., 2017), ethanol (ET) (Schouten et al., 1998) and respiratory quotient (RQ) (Weber et al., 2015; Both et al., 2017). However, in CF- and ET-based DCA, a less accurate detection of the low O_2 level may occur by a result of non-O_2 stress triggers of chlorophyll fluorescence (Wright et al., 2010) and the high solubility of ethanol in aqueous environments (Gupta et al., 2000), respectively. Bessemans et al. (2016; 2020) used the RQ as an indicator, which is calculated as the ratio of the CO_2 production to the O_2 consumption rate. In fermentation conditions this ratio

drastically increases to a value much larger than 1. Which value of RQ is critical, is a subject of debate.

Since invasive measurement of internal gas concentrations in tissues is destructive, models that predict the internal gas concentration gradients inside pear fruit are helpful to improve our understanding of hypoxic responses of pear fruit in very low oxygen conditions such as during DCA storage. Bessemans et al. (2020) developed a lumped three-compartment model to describe the rate of O_2 consumption and CO_2 production and RQ at the cellular level, which assumed that the pear skin is the main resistance to gas exchange, ignoring the resistance caused by the porous network of intercellular gas spaces. Still, they found a difference between the actual RQ levels of cells in the pear fruit and the one calculated from the gas concentration changes in the storage atmosphere. The difference increased as the applied O_2 partial pressure decreased. Delele et al. (2019) also showed that internal RQ levels could be significantly different from those calculated from the storage atomosphere conditions.

Because of the internal resistance to gas transport the actual O_2 partial pressure and internal RQ are spatially distributed. The above models are lumped and cannot be used to predict such spatial gradients. A multiscale gas exchange model was developed by Ho et al. (2011; 2013) to predict O_2 and CO_2 concentration profiles in pome fruit. Gas-transport properties of tissue, such as the effective O_2 and CO_2 diffusivities, are computed with a microscale gas transport model that incorporates the detailed microscale geometry of the tissue. A gas exchange model operating at the macroscale level of the whole fruit incorporates these properties to predict the internal gas profiles. However, because the gas transport properties are not homogenous over the fruit due to the complex structure of the tissue (Janssen et al., 2020), the implementation of a uniform effective diffusivity may cause prediction errors of gas concentrations and local respiration and fermentation rates. A comprehensive computation of the gas exchange incorporating heterogeneous spatially dependent properties is required to explore the onset of internal disorders as affected by very low oxygen storage conditions under DCA. Significant

efforts have been conducted to predict and map the spatial distribution of tissue porosity across a fruit using non-destructive imaging methods such as X-ray computed tomography (CT) (Tanaka et al., 2018; Nugraha et al., 2019; Chigwaya et al., 2021) or magnetic resonance imaging (MRI) (Musse et al., 2010; Winisdorffer et al., 2015). In a further step, the X-ray CT-based method of porosity mapping (Nugraha et al., 2019) was successfully extended to predict the effective O_2 diffusivity distribution (Nugraha et al., 2021).

This work aims to explore the internal gas concentration and RQ profiles in pear fruit stored under very low oxygen concentrations using a gas transport model that incorporates 3-D effective diffusivity maps. The effect of incorporating the heterogeneous diffusivity on local respiration and fermentation rates will be investigated. The simulated contours of O_2, CO_2 and RQ concentrations inside the pear will be related to the incidence of internal browning of pears after storage in internal browning-inducing CA conditions. As the purpose of the work was to demonstrate the correspondence of prediction to observation on individual fruit, a limited number of fruit with different shapes and diffusivity distribution were used in this study.

2 Materials and methods

2.1 Pear fruit

'Conference' pears (*Pyrus communis* L. cv. Conference) were picked on 9th of September 2019, in a commercial orchard in Kortenaken, Belgium (50°53'07.0"N 5°01'34.0"E), more than two weeks after the optimal commercial picking date (August 23) predicted by the Flanders Centre of Postharvest Technology (Leuven, Belgium). Late picked pears were used to increase the susceptibility to browning development, as reported by Lammertyn et al. (2000) and Ho et al. (2016). Four fruit were immediately scanned using X-ray Computed Tomography (CT) to obtain the shape and porosity map of the intact fruit. The scanned fruit were then stored in very low oxygen conditions (1 kPa O_2; 0.7 kPa CO_2 at 1 ^oC) without a pre-cooling period in the pilot

facility of the Flanders Centre of Postharvest Technology (Leuven, Belgium). Such conditions increase the likelihood of inducing browning disorders (Lammertyn et al., 2000). The other 30 fruit were directly stored under the same conditions for intermediate internal browning checks every 2 month. After 4 months of storage, the O_2 concentration was lowered to 0.5 kPa, because no browning incidence was yet observed. Internal browning eventually was observed after 8 months of storage. The four test pears were scanned again using the same setting of the X-ray CT to determine the browning-affected regions of the pear. The scanned pears were cut into 5 mm thick cross-sectional slices and photographed to visualize the incidence of internal browning.

2.2 X-ray CT scans and 3-D pear geometry construction

Pear samples were scanned at low resolution (86 µm isotropic voxel size) using the in-house developed X-ray CT scanner HECTOR of the Ghent University Centre for Tomography (UGCT) (Masschaele et al., 2013). Once the set resolution was larger than the size of cells and pores, the CT image of intact pear tissue would only be presented by the grayscale intensities that corresponded to the heterogeneity of the internal tissue density, dependent on tissue porosity, due to the partial volume effect. Using the tube settings of 120 kV and 20 W target power (180 µA tube current), the effect of the focal spot on the spatial resolution was negligible. Covering a rotation of 360°, 1800 projection images at an exposure time of 666 ms each were acquired. The projection data were reconstructed into 3D volumes using the Octopus reconstruction software (Octopus Imaging Software. Ghent, Belgium). Filtered pear juice in a small tube was scanned along with an entire pear as a zero porosity reference for tissue porosity mapping as described by Nugraha et al. (2019).

For image processing, the reconstructed CT images were then imported in Avizo Fire Edition 2019.3 (VSG, Bordeaux, France). The CT images of the same pear fruit were aligned to one another using the image registration module in Avizo. The pear volume and its background

(air) were then segmented using Otsu's thresholding to produce binary mask images. Small water phantoms scanned along with the sample and tape were then removed manually. Some tiny spots not recognized as tissue during mask binarization were closed by a filling operation to include them in the pear volume. For the affected pears, the cavities were sufficiently segmented by means of Otsu's thresholding as they had similar intensities to the background. Masking of the original grayscale CT image was performed to clean away materials such as tape and Styrofoam in the background. The stacks of the cleaned CT images were then imported in Matlab 19.a (The Mathworks, Inc., Natick, MA) for mapping of porosity and effective diffusivity.

The real 3D shape of pear was created from the binary image using a 'generate surface' module in Avizo and exported as an STL-file. Detailed air fractions in the middle of the pear (core) were removed to simplify the pear geometry, as these features will be represented by the porosity map. In the next step, a surface mesh was created in ICEM CFD 19.2 (ANSYS Inc., Canonsburg, PA, USA) and then imported in COMSOL Multiphysics 5.5 (COMSOL Inc., Stockholm, Sweden). The surface meshes were then transformed into a volume finite element mesh for the respiratory gas transport simulations.

2.3 Mapping of effective O_2 diffusivities

In Matlab, the grayscale values of the CT images were initially translated to total porosity using the mapping technique developed by Nugraha et al. (2019). As effective O_2 diffusivity correlates better with open porosity, the total porosity map ε was transformed to open porosity map ε_o using a open-total porosity regression formula (Nugraha et al., 2021):

$$\varepsilon_o = a\varepsilon^b \quad (1)$$

where a (0.25) and b (1.66) are fitting parameters. The open porosity map of pear was subsequently translated to the effective O_2 diffusivity map $D_{O_2,eff}$ using the following equation (Nugraha et al., 2021):

$$D_{O_2,eff} = \varepsilon_o{}^n D_{O_2,g} + (1-\varepsilon_o) D_{O_2,l,eff} \quad (2)$$

The first and second term in the right hand side of Equation (2) are the O_2 diffusivity in the (connected) intercellular spaces and in the cells (including trapped pores), respectively; $D_{O_2,g}$ ($m^2\ s^{-1}$) is the O_2 diffusivity in air; n a model fitting parameter to account for pore geometry effects; and $D_{O_2,l,eff}$ ($m^2\ s^{-1}$) is the effective O_2 diffusivity in a trapped (closed)-pore tissue based on the Maxwell-Garnet model (Kalnin et al., 2002):

$$D_{O_2,l,eff} = D_{O_2,l} RTH_{O_2} \left(1 + \frac{3\left(D_{O_2,g} - D_{O_2,l} RTH_{O_2}\right)\varepsilon_{c,l}}{D_{O_2,g} + 2D_{O_2,l} RTH_{O_2} - \left(D_{O_2,g} - D_{O_2,l} RTH_{O_2}\right)\varepsilon_{c,l}} \right) \quad (3)$$

with R ($J\ mol^{-1}\ K^{-1}$) the universal gas constant, T (K) temperature and H_{O_2} ($mol\ m^{-3}\ kPa^{-1}$) Henry's constant for O_2 equilibrium between water and air. $\varepsilon_{c,l}$ is the porosity calculated for the tissue without open pores:

$$\varepsilon_{c,l} = \frac{\varepsilon_c}{1-\varepsilon_o} \quad (4)$$

with ε_c the closed porosity. The affected pears consisted of damaged and sound tissue. The effective O_2 diffusivity in the damaged tissue area with high porosity (> 8%) was predicted using the total porosity-based model (Nugraha et al., 2021):

$$D_{O_2,eff} = \varepsilon^n D_{O_2,g} + (1-\varepsilon) D_{O_2,l} RTH_{O_2} \quad (5)$$

2.4 Mapping of effective CO_2 diffusivities

The effective CO_2 diffusivity was mapped using a regression model of the effective CO_2 diffusivity as function of the O_2 diffusivity (Figure 1) computed previously using a microscale

model (Ho et al., 2016). The regression showed that the CO_2 diffusivity linearly increased with increasing O_2 diffusivity, with generally higher values because of the higher solubility of CO_2 in the liquid phase. The resulting linear regression model was expressed as:

$$D_{CO_2,eff} = mD_{O_2,eff} + n \qquad (6)$$

where $D_{CO_2,eff}$ and $D_{O_2,eff}$ ($m^2\ s^{-1}$) are the effective diffusivities of CO_2 and O_2, respectively, and with m (0.87) the gradient and n ($9.61\times10^{-9}\ m^2\ s^{-1}$) the intercept values. The fitting line has an $R^2 = 0.97$ and RMSE = $5.51\times10^{-10}\ m^2\ s^{-1}$.

2.5 Internal browning segmentation

The tissue patches in the pears subjected to internal browning inducing conditions were classified into three types: sound tissue, brown tissue and cavity. The brown tissue and cavity together form the total affected tissue. The cavity, the air fraction, could be simply segmented from the original CT images as its contrast was excellent. However, due to insufficient contrast between the browning and sound tissue area, segmentation of the brown tissue volume was performed by mapping the relative difference between the calculated porosity of the affected pear and the calculated porosity of the same pear before storage (heathy pear), divided by the calculated porosity of the healthy pear. Where this difference was large, it was assumed that this indicated considerable tissue changes during storage, and the corresponding patch was then segmented as affected (brown + cavities) tissue. The threshold value was selected such that the percentage of the affected patch obtained after segmentation corresponded to that in the photograph. The area of both patches was statistically compared by means of a t-test at a significant level of 5 %. The brown tissue was then the difference between the total affected tissue and cavity. The volume of the intact pear, brown patches and cavities was then calculated and visualized.

2.6 Macroscale gas exchange model for intact pear

A reaction-diffusion model previously developed by Ho et al. (2006b, 2010) was used to compute the overall gas exchange in intact fruit for the applied external gas conditions. The effect of permeation (transport caused by pressure gradients due to different diffusion fluxes of O_2 and CO_2, see Ho et al. (2006b)) was initially tested using the regular gas exchange model (Ho et al., 2011) and was found to hardly affect the predicted O_2 concentration inside the fruit (Supplementary 1) and thus neglected. The simplified model could then be rewritten as:

$$\alpha_i \frac{\partial C_i}{\partial t} = \nabla \cdot D_{i,eff} \nabla C_i + R_i \quad (7)$$

with α_i the gas capacity of component i (O_2 and CO_2) of tissue, C_i (μmol m^{-3}) concentration of O_2 or CO_2, t (s) time, $D_{i,eff}$ (m^2 s^{-1}) apparent diffusivity, R_i (mol m^{-3} s^{-1}) consumption and production terms of O_2 and CO_2, respectively, and ∇ (m^{-1}) the gradient operator. The gas capacity α_i was described as (Ho et al., 2006b; 2011):

$$\alpha_i = \varepsilon_t + (1-\varepsilon_t) RTH_i = \frac{C_{i,tissue}}{C_i} \quad (8)$$

where ε is the fractional porosity of tissue and $C_{i,g}$ (μmol m^{-3}) and $C_{i,tissue}$ (μmol m^{-3}) are the gas concentration of i in the gas phase and tissue, respectively. The concentration of gas molecules in the liquid phase of the tissue follows Henry's law represented by the constant H_i (mol m^{-3} Pa^{-1}) with R (J mol^{-1} K^{-1}) and T (K) as the universal gas constant and temperature, respectively.

A non-competitive inhibition model (Peppelenbos and Leven, 1996a; Hertog et al., 1998; Lammertyn et al., 2001; Ho et al., 2011) was used to describe O_2 consumption by respiration:

$$R_{O_2} = -\frac{V_{m,O_2} C_{O_2}}{\left(K_{m,O_2} + C_{O_2}\right)\left(1 + \frac{C_{CO_2}}{K_{mn,CO_2}}\right)} \quad (9)$$

with V_{m,O_2} (mol m^{-3} s^{-1}) the maximum oxygen consumption rate, C_{O_2} (mol m^{-3}) the O_2 concentration, K_{m,O_2} (mol m^{-3}) the Michaelis-Menten constant for O_2 consumption, K_{mn,CO_2} (mol m^{-3}) the Michaelis-Menten constant for non-competitive CO_2 inhibition, and R_{O_2} (mol m^{-3} s^{-1}) the O_2 consumption rate of the sample.

The production rate of CO_2 that consists of an oxidative respiration part and a fermentative part is described as follows (Peppelenbos et al., 1996b):

$$R_{CO_2} = -r_{q,ox} R_{O_2} + \frac{V_{m,f,CO_2}}{\left(1 + \frac{C_{O_2}}{K_{m,f,O_2}}\right)} \quad (10)$$

with V_{m,f,CO_2} (mol m^{-3} s^{-1}) maximal fermentative CO_2 production rate of the tissue, (mol m^{-3}), K_{m,f,O_2} (mol m^{-3}) the Michaelis-Menten constant for the inhibition of O_2 on fermentative CO_2 production, $r_{q,ox}$ the respiration quotient at high O_2 concentrations and R_{CO_2} (mol m^{-3} s^{-1}) the CO_2 production rate of the sample.

The following boundary condition of the fruit is implemented at the surface:

$$-D_i \frac{\partial C_i}{\partial n} = h_i (C_i - C_{i,\infty}) \quad (11)$$

with n the outward normal to the surface; the index ∞ referring to the gas concentration of the ambient atmosphere; and h_i (m s^{-1}) the skin permeability for gas i. The permeability of the pear skin calculated by Ho et al. (2018) was used in this study.

Model parameters are given in Table 1. The maximal respiration rate of O_2 consumption, V_{m,O_2}, and the CO_2 production rate, V_{m,f,CO_2}, are known to be affected by harvest date: late-harvested pear fruit typically have a higher maximal respiration rate than early- or optimally harvested pear (Ho et al., 2016). The respiration kinetics of late-picked pears estimated by Ho et al. (2016) are, therefore, appropriate for the late-picked pears used in this study.

Table 1. Parameters of the respiration-diffusion model of late picked 'Conference' pears

Constants	O_2	CO_2	Description
$D_{i,eff}$	O_2 diffusivity map (1)	CO_2 diffusivity map (1)	Effective diffusivity
h_i	6.74×10^{-6} m s^{-1} (2)	10.2×10^{-7} m s^{-1} (2)	Skin permeability
K_{m,O_2}	0.17 kPa (3)		Michaelis-Menten constant for O_2 consumption
K_{mn,CO_2}		66.4 kPa (4)	Michaelis-menten constant for non-competitive CO_2 inhibition
K_{m,f,O_2}		0.024 kPa (3)	Michaelis-Menten constant of O_2 inhibition on fermentative CO_2 production
V_{m,O_2}	2.23×10^{-5} mol m^{-3} s^{-1} (2)		Maximum O_2 consumption of late picked pear at 0 ^oC
V_{m,f,CO_2}		1.90×10^{-5} mol m^{-3} s^{-1} (2)	Maximum CO_2 fermentative production rate of late picked pear at 0 ^oC
rq_{ox}		0.77 (2)	Respiratory quotient at high O_2 partial pressure
$E_{a,V_{m,O_2}}$	73 kJ mol^{-1} (4)		Activation energy of O_2 consumption
$E_{a,V_{m,f,CO_2}}$		58.5 kJ mol^{-1} (4)	Activation energy of CO_2 consumption

(1) obtained from the diffusivity map procedure of four pears; (2) Ho et al. (2018); (3) Ho et al. (2013b); (4) Ho et al. (2008).

2.7 Gas exchange simulation using heterogeneous effective diffusivity

The diffusivity maps were firstly resized to increase the computational efficiency by binning 10 voxels by means of a linear interpolation procedure in Matlab. This allowed to speed up the

simulation process without affecting the results significantly (Supplementary 2). The binned map of the diffusivity was then uploaded to Comsol multiphysics 5.5. The lower and upper limits of the physical x-y-z coordinates of the map were set as input arguments. The diffusivity maps were then integrated into the STL geometry file, and the macroscale gas exchange model was then discretized using the finite element method. The effective diffusivity values at every integration point in the finite element mesh was then calculated using a built-in interpolation function. As a comparison, gas exchange simulations using a uniform diffusivity for O_2 and CO_2 were performed. The uniform diffusivity was an average of the values in the entire map. Since the simulation was performed at 1 ^oC (the storage condition), the effect of temperature on the maximal respiration rate (V_{m,O_2}, and V_{m,f,CO_2}) was estimated using Arrhenius' equation as proposed by Ho et al. (2010; 2018).

2.8 Critical oxygen level

The incidence of internal browning after storage was assumed to be associated with hypoxic conditions that could be predicted by the gas transport model and corresponding RQ values inside the pear. When the internal O_2 concentration drops below a threshold, fermentation rather than aerobic respiration is expected to occur (Gran and Beaudry, 1993; Ho et al., 2013; 2016; Xiao et al., 2018). This condition has been suggested as a trigger of internal browning (Ho et al., 2016). Different approaches to estimate the low O_2 limit have been proposed. Ho et al. (2013) estimated the critical limit based on energy supply criteria where the ATP production rate by aerobic respiration was equal to the maximum ATP production by fermentation (assuming no upregulation of glycolysis). The critical O_2 limit, $C_{O_2}^*$ (kPa), is then given by:

$$C_{O_2}^* = \frac{f_f V_{m,f,CO_2} K_{m,O_2}}{f_o V_{m,O_2} r_{q,ox} - f_f V_{m,f,CO_2}} \quad (12)$$

where f_o and f_f are the stoichiometric coefficients of the ATP production due to oxidative respiration and fermentation, respectively. In aerobic respiration, one glucose molecule generally produces 38 ATP molecules and 6 CO_2 molecules, so that f_o is 38/6 = 6.33. In fermentation, one glucose molecule produces 2 ATP molecules and 2 molecules of CO_2, so that f_f is 2/2 = 1. The lowest predicted O_2 level inside the fruit was then compared to the $C^*_{O_2}$ (kPa).

Another method is based on the increase in the respiratory quotient (RQ) resulting from a drop in the O_2 concentration (Beaudry, 1993; Gran and Beaudry, 1993; Saenmuang et al., 2012). Here we calculated and mapped the internal RQ by using the respiration models (Equation 9 and 10) with the predicted O_2 and CO_2 concentrations inside the pear as input, i.e.:

$$RQ = \frac{R_{CO_2}}{R_{O_2}} \quad (13)$$

where RQ represents the tissue respiratory quotient.

The value of the RQ exponentially increases below the lower O_2 limit. In this study, the RQ limit (RQ^*) was calculated by substituting $C^*_{O_2}$ (kPa) into the respiration rate model for O_2 and CO_2 (Equation 9 and 10). In this way, the relatively small inhibition effect of the CO_2 concentration (Equation 9) was ignored. From the internal RQ and O_2 concentration predictions, RQ values along the radial axis of the pear were plotted against O_2 concentrations at the same location to visualize the change of internal RQ as a function of the internal O_2 level.

3 Results

3.1 Incidence of internal breakdown after storage

Development of internal browning was observed after 8 months of storage (Figure 2A, B, C and D). The distribution and shape of the affected tissue varied spatially within and among pear

fruit; the symptoms even extended to the neck part in pear 2. The cavities that developed after browning occurred locally with varying volumes throughout the pear. Only tissue close to the skin remained unaffected.

Figures 2E, F, G and H represent vertical and horizontal slices from grayscale CT image of the pears. The horizontal slices were approximately taken from the largest cross-sectional area of the pear. The darker areas in the cortex tissue were assigned as browning-affected tissue (i.e., zones with lower porosity), while the black pixels specifically indicate cavities (the highest porosity). Figures 2I, K and L show the corresponding photographs of pear slices in which the affected tissue region is clearly visible except for pear 2 (Figure 2J). The cavities were less visible in the pear photographs. Differences between CT slices and photographs were most likely due to the slight density change in the affected tissue and liquid-filled pores at the core region which was initially already dense. While the core tissue actually became brown after storage, this change could not be distinguished from the CT image intensity based on tissue density alone. Therefore, segmentation only relying on the CT image of the affected pear may underestimate the browning in low porosity zones where the porosity increase is not significant.

A volumetric analysis of the volume and percentage of the affected tissue, brown tissue, and cavities is summarized in Table 2. The volume of the affected tissue was defined as the sum of the volumes of the brown tissue and cavities in the slices. The percentages of the affected tissue based on either the relative change in porosity map or photograph were similar.

Surprisingly, there was no relation between the total volume of the pear and that of the affected tissue. Pear 4 and 3 were the smallest and had the smallest (18 %) and largest (34 %) volume percentage of affected tissue, respectively. The volume of affected tissue was also not related to the total volume of the pear in case of cavity formation. The largest cavity was found in pear 2, corresponding to 0.31 % of the total sample volume.

Table 2. Volumetric analysis of browning disorder in pear, with *V* the volume of the pear sample, and *P* their percentage relative to the volume of the entire pear.

Sample	$V_p\ (cm^3)$	$V_{at}\ (cm^3)$	$V_b\ (cm^3)$	$V_c\ (cm^3)$	$P_{at}\ (\%)$	$P_b\ (\%)$	$P_c\ (\%)$	$P_{at}^*\ (\%)$
1	294.2	64.00	63.78	0.21	21.75	21.68	0.07	21.34
2	333.4	80.55	79.50	1.05	24.16	23.85	0.31	20.67
3	272.2	92.42	92.39	0.03	33.95	33.94	0.01	36.01
4	260.3	46.92	46.55	0.37	18.03	17.89	0.14	16.66

subscripts: *p* = pear; *at* = affected tissue; *b* = brown tissue; *c* = cavities;
superscript: * = area fraction from the photograph. No statistical difference between P_{at} and P_{at}^* ($p > 0.05$).

3.2 Map of effective O_2 and CO_2 diffusivities

The effective diffusivity of O_2 in intact pear was lower than that of CO_2, but the spatial distribution of the O_2 and CO_2 diffusivity was similar due to their linear correlation (Figure 3). The porosity maps can be found in Supplementary 3. In sound pears, larger values of effective O_2 and CO_2 diffusivity were mostly located in the cortex tissue, while the smaller values were located near the skin, and in the core and neck region (Figure 3). Overall, pear 4 (Figure 3D and H) had a larger effective O_2 and CO_2 diffusivity compared to the other samples that were very similar. From Figure 3 it can be seen that pear 4 has higher diffusivity values in the cortex of equatorial region of the fruit than for the other fruit. This is a result of a higher porosity of the tissue, which is also reflected in the value given in Table 2

After 8-months storage, the severe development of browning and cavities considerably altered the effective diffusivity of O_2 and CO_2 (Figure 4) to be higher and lower in certain areas relative to that of sound pear. This was most likely due to the presence of cavities (higher) or liquid-filled pore spaces (lower) due to internal breakdown. The maximum diffusivity was identical to that of O_2 and CO_2 in the air inside the cavities.

The mean porosity, effective O_2 and CO_2 diffusivities in each pear and for each condition are presented in Table 3. There was a considerable difference between the values of these

properties in sound and affected tissue. The development of browning and cavities after 8-months storage caused changes in the porosity of the fruit. This is especially clear in pear 2, which had the largest volume of brown patches and cavities of all affected pear fruit (Table 2). Given the mean values are averages of the spatial distributions of individual fruit, it is, however, not possible to test the statistical significance of these differences in a straightforward way.

Table 1. Mean value (± standard deviation) of porosity, O_2 and CO_2 diffusivity.

Sample	Condition	ε_{mean} (%)	$D_{O_2,eff,mean}$ ($\times 10^{-8}$ m^2 s^{-1})	$D_{CO_2,eff,mean}$ ($\times 10^{-8}$ m^2 s^{-1})
1	Sound	4.27 ± 1.10	2.65 ± 1.70	3.29 ± 1.49
	Affected	4.95 ± 2.47	5.04 ± 15.7	5.38 ± 13.7
2	Sound	4.20 ± 1.09	2.54 ± 1.64	3.19 ± 1.44
	Affected	5.41 ± 5.00	9.24 ± 63.9	9.07 ± 56.1
3	Sound	4.09 ± 1.07	2.33 ± 1.47	3.01 ± 1.29
	Affected	4.87 ± 1.98	4.65 ± 6.50	5.04 ± 5.70
4	Sound	4.75 ± 1.22	3.68 ± 2.25	4.19 ± 1.97
	Affected	5.53 ± 3.07	6.78 ± 16.1	6.91 ± 1.41

3.3 Gas exchange simulations

Here we present the distribution of respiratory gasses in fruit that was simulated by taking into account the spatial distribution of diffusivity in the pears. The internal O_2 and CO_2, concentration and RQ profiles are given for the storage condition of 1.0 kPa O_2, 0.7 kPa CO_2 at 1 ^oC and 0.5 kPa O_2, 0.7 kPa CO_2 at 1^oC. As a comparison, reference O_2 and CO_2 concentration and RQ profiles were computed using a uniform (average) O_2 and CO_2 diffusivity. The prediction results are then interpreted with respect to the incidence of internal browning found after storage.

The internal O_2 (Figure 5A, B, C and D) and CO_2 (Figure 5E, F, G and H) concentrations decreased and increased towards the pear center, respectively. Minimal O_2 concentrations were

around 0.10 kPa for pear 1, 2 and 3. For pear 4, the minimal O_2 concentration was higher (0.17 kPa) than the concentration in other pear samples (Figure 5D). No strong gradient in RQ level was observed inside the pears (Figure 5I, J, K and L). The RQ levels were slightly higher in the core region with a maximal value of 1.0-1.7.

Since there was no internal browning found at 1.0 kPa O_2 after the first 4-month storage period, the O_2 level in the storage headspace was decreased to 0.50 kPa O_2. Given that the other parameters were the same, the simulation results are shown in Figure 6. Compared to the simulation results at 1.0 kPa O_2, the internal O_2 level calculated under 0.5 kPa O_2 condition dropped below 0.1 kPa with slight gradients from the outer to inner parts (Figure 6A, B, C and D). The CO_2 concentration at the center was greater than that at the periphery (Figure 6E, F, G and H). The internal RQ levels increased considerably above 1 towards the core region (Figure 6I, J, K and L) at which the O_2 and CO_2 partial pressures were found minimal and maximal, respectively. The internal RQ gradient was less steep in pear 4 (1.0 – 2.7) which had a larger O_2 and CO_2 diffusivity (Figure 3D and H). The results confirm that differences in tissue porosity (Supplementary 3) and, thus, O_2 and CO_2 diffusivity of sound pears (Figure 3), may partially explain differences in internal gas gradients (Figure 5 and 6).

Different results were found in model simulations based on a homogenous diffusivity for both O_2 and CO_2 (Figure 7). The internal O_2 and CO_2 concentration and RQ profiles were more uniform across the entire pear tissue than those computed using the diffusivity map of O_2 and CO_2. The internal RQ levels that were predicted remained around 1 (aerobic respiration) in all tissue positions suggesting that development of internal browning or cavities would be unlikely (Figure 7I, J, K and L). This is in contrast with the observed internal browning after storage.

3.4 Heterogeneous versus uniform diffusivity

The difference between the O_2 and CO_2 concentration and RQ profiles computed using heterogeneous and homogeneous O_2 and CO_2 diffusivity were divided by the latter to obtain relative difference profiles. A negative or positive sign indicates that the predictions using heterogeneous diffusivities were lower or higher, respectively, than those obtained with a uniform diffusivity. At the fruit skin the concentration computed with heterogeneous gas diffusivities was 30 to 50 % larger than that computed with the uniform gas diffusivities, while at the fruit center they were 80 to 60 % smaller (Figure 8A). In contrast, the CO_2 concentration computed using heterogeneous gas diffusivities was 8 to 20 % larger when computed using uniform diffusivities at the pear center (Figure 8B). The relative differences were smaller compared to those for the O_2 profile. A considerable relative difference was observed for the respiratory quotient (RQ). At the center, the values computed using heterogeneous gas diffusivities were around 240 % higher than those computed using uniform gas diffusivities, except for pear 4 (120 %) (Figure 8C).

3.5 Critical O_2 limit and internal browning occurrence

The critical O_2 limit was estimated to explain the occurrence of internal browning based on the simulation results. From the prediction results, the minimal O_2 concentrations in pear 1, 2, 3 and 4 were found to be 0.017 kPa, 0.018 kPa, 0.006 kPa and 0.035 kPa, respectively. Except for pear 4, the lowest O_2 levels were all below the calculated critical O_2 limit ($C^*_{O_2}$) of 0.034 kPa, assuming $f_o = 6.33$. This value assumes a maximal yield of the respiration pathway (38 ATP), which is hardly ever reached due to the complexity of the respiratory chain and the ATP synthase mechanisms (Rich, 2003). A more realistic range is from 30 to 32 ATP, corresponding to f_o = 30/6 = 5 (Edwards et al., 2012). With this value, the estimated $C^*_{O_2}$ was 0.044 kPa, still well above the lowest O_2 concentration in all four pears.

438 At 1.0 kPa O_2, a slight increase of the RQ level occurred as the O_2 concentration decreased
439 from 0.45 to 0.07 kPa (Figure 9A). The RQ levels were mostly below 1, indicating an aerobic
440 condition. At 0.5 kPa O_2, an exponential increase in the RQ levels was observed, while the
441 internal O_2 level dropped below the $C^*_{O_2}$ of 0.044 kPa (Figure 9B) at which the critical RQ limit
442 (RQ^*) was 2.12.
443 The region at which the RQ level was above the aforementioned limit was approximately
444 comparable to the area of the brown patches (Figure 10). When fermentation was predicted
445 assuming heterogeneous gas diffusivities, this did not necessarily mean that the predicted
446 fermentation area would become brown. As the gas exchange simulation was only conducted
447 on sound pears, some local incidences which occurred outside the fermentation area were most
448 likely caused by the development of browning during low O_2 storage. Neither the internal O_2
449 concentrations nor RQ levels simulated using homogeneous gas diffusivities predicted the
450 incidence of internal browning, the minimal O_2 concentration and/or maximal RQ level of all
451 pears were well above or below the critical thresholds, respectively.
452

453 # 4 Discussion

454 Accurate simulation of the metabolic gas composition in stored fruit can be greatly beneficial
455 for understanding and improving CA or DCA storage applications. However, the multiscale
456 modeling approach previously developed assumes a homogeneous microstructure and, hence,
457 homogeneous gas diffusion properties. It may, therefore, not be accurate in predicting the
458 internal gas concentrations since the microstructure of the fruit tissue is not uniform over the
459 entire organ (Ho et al., 2011). Low availability of O_2 in plant tissues may be caused by their
460 large diffusion resistance for O_2 (Gran and Beaudry, 1993; Geigenberger, 2003; van Dongen et
461 al., 2011; Ho et al., 2013). In this study, effective O_2 diffusivity was quantified and visualized
462 in pear fruit based on X-ray CT images using the technique of the diffusivity map developed

463 by Nugraha et al. (2021) while effective CO_2 diffusivity was mapped from the O_2 diffusivity
464 map using the linear regression model (Equation 6). A large variation in the O_2 and CO_2
465 diffusivity within a fruit or among the individual pears reflects the heterogeneity in the tissue
466 microstructure (Figure 3). A variation of gas diffusivity along the pear radial axis was
467 previously observed by Schotsmans et al. (2003). Variations in pear shape and size, the amount
468 of lignified cells, cell distribution and growing conditions all contribute to the biological
469 variability in gas diffusivity (Ho et al., 2006a).
470 This study integrated the spatial variability in the O_2 and CO_2 diffusivity into an existing gas
471 exchange model developed by Ho et al. (2006b, 2008, 2010a, 2011) to predict the local O_2 and
472 CO_2 concentrations inside the pear. Also, the respiratory quotient (RQ) used as a low O_2 stress
473 signal in dynamic controlled atmosphere (DCA) (Weber et al., 2015; Both et al., 2017;
474 Bessemans et al., 2016, 2020) was, for the first time, predicted and mapped in an entire pear
475 organ. The distribution of internal gas concentrations and RQ level followed the spatial
476 variation of the effective O_2 and CO_2 diffusivity and depended on the external gas conditions
477 (Figure 5 and 6). Furthermore, at 0.5 kPa O_2, depletion of O_2 and an increase of the CO_2
478 concentration and RQ levels were steeper (Figure 6) than when a homogeneous O_2 and CO_2
479 diffusivity was assumed (Figure 7), caused by areas of low diffusivity in the core.
480 The internal gas concentration plays a vital role in fruit respiration (Yearsley et al., 1996;
481 Lammertyn et al., 2003a; Xiao et al., 2018), and, hence, the energy availability for cell
482 membrane maintenance (Lammertyn et al., 2003a; Saquet et al., 2003; van Dongen et al.,
483 2011). Excessively low oxygen availability in the tissue may replace aerobic respiration to
484 fermentation, leading to a reduced supply of ATP for energy-demanding activities (Drew,
485 1997; Boeckx et al., 2019). Eventhough cells can temporarily adapt to a low availability of
486 metabolic energy (Drew, 1997; Toro and Pinto, 2015), they may lose membrane integrity after
487 a certain period of time (Rawyler et al., 1999). For ‘Conference’ pear, incidence of internal
488 disorders in relation to limited availability of energy was already observed by Veltman et al.

(2003) and Saquet et al. (2003). We followed a mechanistic approach based on the supply energy criteria (Ho et al,. 2013b) to determine the critical O_2 limit at which the respiration-to-fermentation switch occurs. The critical O_2 limit (0.044 kPa) did correspond approximately to an RQ of 2.12 inside the pear.

The predicted oxygen and RQ levels did not exceed the critical O_2 or the critical RQ limits, respectively, for storage under 1.0 kPa O_2 (Figure 9A). This explains the absence of internal browning inside the test samples after 4 months of storage. When the storage O_2 partial pressure was decreased to 0.5 kPa, the internal O_2 and RQ gradients in all pears crossed the critical thresholds (Figure 9B), indicating insufficient energy for normal cell maintenance of the pear tissue. Previous research found that fermentation occurs when the RQ levels increase above 1.3 (Kader and Saltveit, 2002). The predicted result corresponded to the observation of browning and cavities in the pear samples after storage. Lammertyn et al. (2003c,d) explained that the cytoplasm releases into the intercellular space when the cell membrane integrity loose, locally causing a decrease in porosity. The liquid then gradually diffuses through the pear skin, evaporates and leaves cavities inside the pear. These processes result in an increase in the porosity and diffusivity of the affected pear (Figure 4 and Supplementary 3). Also, these results support the hypothesis that the internal RQ levels are affected by the diffusion resistance (Gran and Beaudry, 1993; Delele et al., 2019; Bessemans et al., 2020). In a future study, the experimental measurement of internal gas concentration is, however, required to validate this improved gas exchange model.

The segmented area beyond the critical RQ limit agreed quite well with the actual area of the affected tissue (Figure 10). The deviation between the predicted and observed areas is most likely due to the fact that the respiration parameters used for the simulation were estimated for sound pears. In disorder-inducing conditions, some tissue regions which did not become brown might have adapted to the limited availability of energy. Later on, the tissue microstructure and, most likely, the respiration activity of pear may change due to the changes caused by the

storage disorder and thus affect internal gas and RQ levels compared to those of sound pear fruit. Investigation of gas transport in browning-affected pear fruit is, therefore, required in future research.

Besides the morphology of the pore structure and diffusion resistance, the high incidence of browning and cavities, as observed in all investigated pears, was most likely affected by the late harvest date. Franck et al. (2007) described that 'Conference' pear fruit harvested at a late harvest date are more susceptible to this disorder than fruit picked at the optimum harvest date. Based on stochastic simulations, Ho et al. (2016) found that the occurrence of browning and cavities is high for late picked pears when stored at an O_2 partial pressure of 0.5 kPa (74 %) and it increases with storage time (1-9 months). The occurrence decreases with increasing applied O_2 in the storage headspace (Ho et al., 2016). The increased susceptibility of late harvested pear is likely due to the higher maximum respiration rate that contributes to the internal gas gradients (Franck et al., 2007; Ho et al., 2016). Temperature also affects the respiration rate of pear as given by the activation energy (Ho et al., 2016; 2018). Hence, temperature is most likely another factor, which exacerbates internal browning since pear fruit is better preserved at -1 °C rather than 1 °C used here. Finally, ripe pears are typically larger than unripe pears and gas transport is highly affected by size.

This work followed a mechanistic approach relying on the physics of diffusion in a porous fruit, while approximating the respiration metabolism by commonly accepted approximations using simplified reaction kinetics. The advantage of this approach is that the effects of the considered processes involved could be assessed independently using their mathematical formulations in a quantitative way. Doing so, we were able to discern the effects of storage conditions on diffusion, respiration and fermentation in a spatially heterogeneous fruit. By only changing the storage conditions from 1 kPa to 0.5 kPa O_2, the model was able to predict consequent changes in the RQ profiles of the fruit, which appeared to correlate well with the occurrence and spatial localization of browning disorder. This does not necessarily mean that

these were the only mechanisms at play in the particular experiment. Conditions were changed during the long-term storage experiment of the fruits. X-ray CT measurements confirmed no changes in the tissue structure after 4 months of storage at 1 kPa, and thus the diffusion properties will not have changed. Still, potentially the particular experimental design could have affected the results by a time effect on the respiratory metabolism through regulation. Consequent changes in respiration kinetics could not be assessed in the current work and are subject of active research in the field of respiratory adaptation (Cukrov et al., 2016; 2018; Xiao et al., 2018; Ho et al., 2018).

We achieved the goal to demonstrate and validate this novel modelling approach that is using diffusivity maps of individual fruit to compute the profiles in respiratory gas concentrations and RQ inside pear fruits, taking into account fruit shape. For this goal, it was sufficient to have a variation in fruit shapes and internal structure using a limited number of fruit, with differences in the responses to very low oxygen, which was the case in this paper. However, to use the methodology to assess, design or optimize entire CA storage rooms operating in (dynamic) controlled atmosphere conditions, the method should be elaborated to account for the variability range of entire fruit batches. Thereto, stochastic approaches should be implemented, accounting for variability in fruit shape, diffusion properties, respiration kinetics and storage conditions and their effect on RQ inside the fruit. Doing so, we will be able to predict confidence levels of optimal conditions and risks for development of internal disorders in specific batches from different origins, picking dates and seasons.

5 Conclusion

Effective O_2 and CO_2 diffusivity maps incorporated into the macroscale model contributed to more realistic O_2 and CO_2 concentration and respiratory quotient profiles inside ‘Conference’ pear fruit that were in line with the local magnitude of the diffusivity distribution. The contours

of critical O_2 concentrations or RQ levels corresponded readily to brown tissue and cavities found after long-term CA storage. Conventional multiscale gas exchange models that assume a homogeneous O_2 and CO_2 diffusivity failed to explain the occurrence of browning and cavities as the predicted gas concentrations indicated a normal aerobic respiration process, even at low oxygen partial pressures.

6 Acknowledgements

This study was supported by KU Leuven (C1 project 3E160393), the Research Council of Norway (project 255596/E50), the Indonesia Endowment Fund for Education (LPDP), Ministry of Finance of The Republic of Indonesia and Universitas Gadjah Mada. The Ghent University Special Research Fund (BOF-UGent) is acknowledged for the financial support of the Centre of Expertise UGCT (BOF.EXP.2017.0007). The opinions expressed in this article do by no means represent the official opinion of the financing bodies or their representatives.

7 References

Beaudry, R.M., 1993. Effect of carbon dioxide partial pressure on blueberry fruit respiration and respiratory quotient. Postharvest Biology and Technology 3, 249–258. https://doi.org/10.1016/0925-5214(93)90060-G.

Bessemans, N., Verboven, P., Verlinden, B.E., Janssens, M., Hertog, M.L.A.T.M., Nicolaï, B.M., 2020. Apparent respiratory quotient observed in headspace of static respirometers underestimates cellular respiratory quotient of pear fruit. Postharvest Biology and Technology 162, 111104. https://doi.org/10.1016/j.postharvbio.2019.111104.

Bessemans, N., Verboven, P., Verlinden, B.E., Nicolaï, B.M., 2016. A novel type of dynamic controlled atmosphere storage based on the respiratory quotient (RQ-DCA). Postharvest Biology and Technology 115, 91–102. https://doi.org/10.1016/j.postharvbio.2015.12.019.

Brady, C.J., Romani, R.J., 1988. Respiration and protein synthesis in nongrowing cultured pear fruit cells in response to ethylene and modified atmospheres: A Model System for Fruits Postharvest. Plant Physiol. 87, 571–576. https://doi.org/10.1104/pp.87.3.571

Chigwaya, K., Karuppanapandian, T., Schoeman, L., Viljoen, D.W., Crouch, I.J., Nugraha, B., Verboven, P., Nicolaï, B.M., Crouch, E.M., 2021. X-ray CT and porosity mapping to determine the effect of 'Fuji' apple morphological and microstructural properties on the incidence of CO_2 induced internal browning. Postharvest Biology and Technology 174, 111464.

Cukrov, D., 2018. Progress toward Understanding the Molecular Basis of Fruit Response to Hypoxia. Plants 7, 78. https://doi.org/10.3390/plants7040078

Cukrov, D., Zermiani, M., Brizzolara, S., Cestaro, A., Licausi, F., Luchinat, C., Santucci, C., Tenori, L., Van Veen, H., Zuccolo, A., Ruperti, B., Tonutti, P., 2016. Extreme Hypoxic Conditions Induce Selective Molecular Responses and Metabolic Reset in Detached Apple Fruit. Front. Plant Sci. 7. https://doi.org/10.3389/fpls.2016.00146

Delele, M.A., Bessemans, N., Gruyters, W., Rogge, S., Janssen, S., Verlinden, B.E., Smeets, B., Ramon, H., Verboven, P., Nicolai, B.M., 2019. Spatial distribution of gas concentrations and RQ in a controlled atmosphere storage container with pear fruit in very low oxygen conditions. Postharvest Biology and Technology 156, 110903. https://doi.org/10.1016/j.postharvbio.2019.05.004

Drew, M.C., 1997. Oxygen deficiency and root metabolism: injury and acclimation under hypoxia and anoxia. Annu. Rev. Plant. Physiol. Plant. Mol. Biol. 48, 223–250. https://doi.org/10.1146/annurev.arplant.48.1.223

Edward, J.M., Roberts, T.H., Atwell, B.J. 2012, Quantifying ATP turnover in anoxic coleoptiles of rice (Oryza sativa) demonstrates preferential allocation of energy to protein synthesis. Journal of Experimental Botany 63, 4389-4402. doi:10.1093/jxb/ers114.

Franck, C., Lammertyn, J., Ho, Q.T., Verboven, P., Verlinden, B., Nicolaï, B.M., 2007a. Browning disorders in pear fruit. Postharvest Biology and Technology 43, 1–13. https://doi.org/10.1016/j.postharvbio.2006.08.008.

Gran, C.D., Beaudry, R.M., 1993. Determination of the low oxygen limit for several commercial apple cultivars by respiratory quotient breakpoint. Postharvest Biology and Technology 3, 259–267. https://doi.org/10.1016/0925-5214(93)90061-7.

Hertog, M.L.A.T.M., Peppelenbos, H.W., Evelo, R.G., Tijskens, L.M.M., 1998. A dynamic and generic model of gas exchange of respiring produce : the effects of oxygen, carbon dioxide and temperature Postharvest Biology and Technology 14, 335–349. https://doi.org/10.1016/S0925-5214(98)00058-1.

Ho, Q.T., Verlinden, B.E., Verboven, P., Nicola, B.M., 2006a. Gas diffusion properties at different positions in the pear. Postharvest Biology and Technology 41, 113–120. https://doi.org/10.1016/j.postharvbio.2006.04.002

Ho, Q.T., Verlinden, B.E., Verboven, P., Vandewalle, S., Leuven, K.U., Computing, S., Leuven, K.U., 2006b. A permeation – diffusion – reaction model of gas transport in cellular tissue of plant materials. Journal of Experimental Botany 57, 4215–4224. https://doi.org/10.1093/jxb/erl198.

Ho, Q.T., Verboven, P., Verlinden, B.E., Lammertyn, J., Vandewalle, S., Nicolaï, B.M., 2008. A Continuum Model for Metabolic Gas Exchange in Pear Fruit. PLoS Computational Biology 4, 13. https://doi.org/10.1371/journal.pcbi.1000023.

Ho, Q.T., Verboven, P., Verlinden, B.E., Nicolaï, B.M., 2010. A model for gas transport in pear fruit at multiple scales. Journal of Experimental Botany 61, 2071–2081. https://doi.org/10.1093/jxb/erq026.

Ho, Q.T., Verboven, P., Verlinden, B.E., Herremans, E., Wevers, M., Carmeliet, J., Nicolaï, B.M., 2011. A three-dimensional multiscale model for gas exchange in fruit. Plant physiology 155, 1158–1168. https://doi.org/10.1104/pp.110.169391.

Ho, Q.T., Verboven, P., Verlinden, B.E., Schenk, A., Nicolaï, B.M., 2013. Controlled atmosphere storage may lead to local ATP deficiency in apple. Postharvest Biology and Technology 78, 103–112. https://doi.org/10.1016/j.postharvbio.2012.12.014.

Ho, Q.T., Rogge, S., Verboven, P., Verlinden, B.E., Nicolaï, B.M., 2016. Stochastic modelling for virtual engineering of controlled atmosphere storage of fruit. Journal of Food Engineering 176, 77–87. https://doi.org/10.1016/j.jfoodeng.2015.07.003.

Ho, Q.T., Hertog, M.L.A.T.M., Verboven, P., Ambaw, A., Rogge, S., Verlinden, B.E., Nicolaï, B.M., 2018. Down-regulation of respiration in pear fruit depends on temperature. Journal of Experimental Botany 69, 2049–2060. https://doi.org/10.1093/jxb/ery031.

Janssen, S., Verboven, P., Nugraha, B., Wang, Z., Boone, M., Josipovic, I., Nicolaï, B.M., 2020. 3D pore structure analysis of intact 'Braeburn' apples using X-ray micro-CT. Postharvest Biology and Technology 159, 111014. https://doi.org/10.1016/j.postharvbio.2019.111014.

Kader, A., Saltveit, M., 2002. Respiration and Gas Exchange, in: Bartz, J. (Ed.), Postharvest Physiology and Pathology of Vegetables. CRC Press. https://doi.org/10.1201/9780203910092.ch2.

Kalnin, J.R., Kotomin, E.A., Maier, J., 2002. Calculations of the effective diffusion coefficient for inhomogeneous media. Journal of Physics and Chemistry of Solids 63, 449–456. https://doi.org/10.1016/S0022-3697(01)00159-7.

Lammertyn, J., Aerts, M., Verlinden, B.E., Schotsmans, W., Nicolaï, B.M., 2000. Logistic regression analysis of factors influencing core breakdown in 'Conference' pears. Postharvest Biology and Technology 20, 25–37. https://doi.org/10.1016/S0925-5214(00)00114-9.

Lammertyn, J., Scheerlinck, N., Verlinden, B.E., Schotsmans, W., Nicolaï, B.M., 2001. Simultaneous determination of oxygen diffusivity and respiration in pear skin and tissue. Postharvest biology and Technology 23, 93–104. https://doi.org/10.1016/S0925-5214(01)00113-2.

Lammertyn, J., Scheerlinck, N., Jancso, P., Verlinden, B.E., Nicolaï, B.M., 2003a. A respiration Á diffusion model for 'Conference' pears I : model development and validation. Postharvest biology and Technology 30, 29–42. https://doi.org/10.1016/S0925-5214(03)00061-9.

Lammertyn, J., Scheerlinck, N., Jancso, P., Verlinden, B.E., Nicolaï, B.M., 2003b. A respiration Á diffusion model for 'Conference' pears II: Simulations and relation to core breakdown Postharvest biology and Technology 30, 43–55. https://doi.org/10.1016/S0925-5214(03)00062-0.

Lammertyn, J., Dresselaers, T., Van Hecke, P., Jancsók, P., Wevers, M., Nicolaï, B.M., 2003c. MRI and x-ray CT study of spatial distribution of core breakdown in 'Conference' pears. Magnetic Resonance Imaging 21, 805–815. https://doi.org/10.1016/S0730-725X(03)00105-X.

Lammertyn, J., Dresselaers, T., Hecke, P. Van, Jancso, P., 2003d. Analysis of the time course of core breakdown in 'Conference' pears by means of MRI and X-ray CT. Postharvest Biology and Technology 29, 19–28. https://doi.org/10.1016/S0925-5214(02)00212-0.

Masschaele, B., Dierick, M., Loo, D. Van, Boone, M.N., 2013. HECTOR : A 240kV micro-CT setup optimized for research 012012. https://doi.org/10.1088/1742-6596/463/1/012012.

Musse, M., De Guio, F., Quellec, S., Cambert, M., Challois, S., Davenel, A., 2010. Quantification of microporosity in fruit by MRI at various magnetic fields: comparison with X-ray microtomography. Magnetic Resonance Imaging 28, 1525–1534. https://doi.org/10.1016/j.mri.2010.06.028.

Nugraha, B., Verboven, P., Janssen, S., Hertog, M.L.A.T.M., Boone, M., Josipovic, I., Nicolaï, B.M., 2021. Oxygen diffusivity mapping of fruit and vegetables based on X-ray CT. Journal of Food Engineering 306, 110640. https://doi.org/10.1016/j.jfoodeng.2021.110640.

Nugraha, B., Verboven, P., Janssen, S., Wang, Z., Nicolaï, B.M., 2019. Postharvest Biology and Technology Non-destructive porosity mapping of fruit and vegetables using X-ray CT. Postharvest Biology and Technology 150, 80–88. https://doi.org/10.1016/j.postharvbio.2018.12.016.

Peppelenbos, H.W., Leven, J. Van, 1996a. Evaluation of four types of inhibition for modelling the influence of carbon dioxide on oxygen consumption of fruits and vegetables. Postharvest Biology and Technology 7, 27–40 https://doi.org/10.1016/0925-5214(96)80995-1.

Peppelenbos, H.W., Tijskens, L.M.M., van 't Leven, J., Wilkinson, E.C., 1996b. Modelling oxidative and fermentative carbon dioxide production of fruits and vegetables. Postharvest Biology and Technology 9, 283–295. https://doi.org/10.1016/S0925-5214(96)00029-4.

Perez, R., Beaudry, R.M., 1998. Fractional surface coating modifies gas diffusion and ripening in bananas. J. Amer. Soc. Hort. Sci 123, 115–118. https://doi.org/10.21273/JASHS.123.1.115

Rajapakse, N.C., Banks, N.H., Hewett, E.W., Cleland, D.J., 1990. Development of oxygen concentration gradients in flesh tissues of bulky plant organs. jashs 115, 793–797. https://doi.org/10.21273/JASHS.115.5.793

753 Rawyler, A., Pavelic, D., Gianinazzi, C., Oberson, J., Braendle, R., 1999. Membrane Lipid
754 Integrity Relies on a Threshold of ATP Production Rate in Potato Cell Cultures
755 Submitted to Anoxia. Plant Physiol. 120, 293–300.
756 https://doi.org/10.1104/pp.120.1.293.
757
758 Rich, P.R., 2003. The molecular machinery of Keilin's respiratory chain. Biochemical Society
759 Transactions 31, 1095–1105. https://doi.org/10.1042/bst0311095.
760
761 Saenmuang, S., Al-Haq, M.I., Samarakoon, H.C., Makino, Y., Kawagoe, Y., Oshita, S., 2012.
762 Evaluation of Models for Spinach Respiratory Metabolism Under Low Oxygen
763 Atmospheres. Food Bioprocess Technol 5, 1950–1962. https://doi.org/10.1007/s11947-
764 010-0503-5.
765
766 Saquet, A.A., Streif, J., Bangerth, F., 2003. Energy metabolism and membrane lipid alterations
767 in relation to brown heart development in 'Conference' pears during delayed controlled
768 atmosphere storage. Postharvest Biology and Technology 30, 123–132.
769 https://doi.org/doi:10.1016/S0925-5214(03)00099-1.
770
771 Tanaka, Fumihiko, Imamura, K., Tanaka, Fumina, Uchino, T., 2018. Determination of thermal
772 diffusivity of persimmon fl esh tissue using three-dimensional structure model based
773 on X-ray computed tomography. Journal of Food Engineering 221, 151–157.
774 https://doi.org/10.1016/j.jfoodeng.2017.10.021.
775
776 Toro, G., Pinto, M., 2015. Plant respiration under low oxygen. Chilean J. Agric. Res. 75, 57–
777 70. https://doi.org/10.4067/S0718-58392015000300007
778
779 van Dongen, J.T., Gupta, K.J., Ramírez-Aguilar, S.J., Araújo, W.L., Nunes-Nesi, A., Fernie,
780 A.R., 2011. Regulation of respiration in plants: A role for alternative metabolic
781 pathways. Journal of Plant Physiology 168, 1434–1443.
782 https://doi.org/10.1016/j.jplph.2010.11.004.
783
784 Winisdorffer, G., Musse, M., Quellec, S., Devaux, M., Lahaye, M., Mariette, F., 2015. MRI
785 investigation of subcellular water compartmentalization and gas distribution in apples
786 Parenchyma Seeds Vascular. Magnetic Resonance Imaging 33, 671–680.
787 https://doi.org/10.1016/j.mri.2015.02.014.
788
789 Xiao, Z., Rogiers, S.Y., Sadras, V.O., Tyerman, S.D., 2018. Hypoxia in grape berries: the role
790 of seed respiration and lenticels on the berry pedicel and the possible link to cell death.
791 Journal of Experimental Botany 69, 2071–2083. https://doi.org/10.1093/jxb/ery039.
792
793 Yearsley, C.W., Banks, N.H., Ganesh, S., Cleland, D.J., 1996. Determination of lower oxygen
794 limits for apple fruit. Postharvest Biology and Technology 8, 95–109.
795 https://doi.org/10.1016/0925-5214(96)00064-6.
796
797 Zhang, J., Bunn, J., 2000. Oxygen diffusivities of apple flesh and skin. Transactions of the
798 ASAE 43, 359–363. https://doi.org/10.13031/2013.2712.
799
800 Both, V., Thewes, F.R., Brackmann, A., de Oliveira Anese, R., de Freitas Ferreira, D., Wagner,
801 R., 2017. Effects of dynamic controlled atmosphere by respiratory quotient on some
802 quality parameters and volatile profile of 'Royal Gala' apple after long-term storage.
803 Food Chemistry 215, 483–492. https://doi.org/10.1016/j.foodchem.2016.08.009.

Gupta, A.K., Teja, A.S., Chai, X.S., Zhu, J.Y., 2000. Henry's constants of n-alkanols (methanol through *n*-hexanol) in water at temperatures between 40 ^{o}C and 90 ^{o}C. Fluid phase equilibria 170, 183-192. doi:http://dx.doi.org/10.1016/s0378-3812(00) 00350-2.

Mditshwa, A., Fawole, O.A., Vries, F., van der Merwe, K., Crouch, E., Opara, U.L., 2017. Minimum exposure period for dynamic controlled atmospheres to control superficial scald in 'Granny Smith' apples for long distance supply chains. Postharvest Biology and Technology 127, 27–34. https://doi.org/10.1016/j.postharvbio.2016.12.009

Prange, R.K., DeLong, J.M., Leyte, J.C., Harrison, P.A., 2002. Oxygen concentration affects chlorophyll fluorescence in chlorophyll-containing fruit. Postharvest Biology and Technology 24, 201–205. https://doi.org/10.1016/S0925-5214(01)00188-0

Schouten, S.P., Prange, R.K., Verschoor, J., Lammers, T.R., Oosterhaven, J., 1998. Improvement of Quality of Elstar Apples by Dynamic Control of ULO Conditions. IFAC Proceedings Vol 31, 25–29. https://doi.org/10.1016/S1474-6670(17)44023-7

Weber, A., Brackmann, A., Both, V., Pavanello, E.P., Anese, R. de O., Thewes, F.R., 2015. Respiratory quotient: innovative method for monitoring 'Royal Gala' apple storage in a dynamic controlled atmosphere. Sci. agric. (Piracicaba, Braz.) 72, 28–33. https://doi.org/10.1590/0103-9016-2013-0429

Wright, H., DeLong, J., Harrison, P.A., Gunawardena, A.H.L.A.N., Prange, R., 2010. The effect of temperature and other factors on chlorophyll a fluorescence and the lower oxygen limit in apples (*Malus domestica*). Postharvest Biology and Technology 55, 21–28. https://doi.org/10.1016/j.postharvbio.2009.07.011

Figures

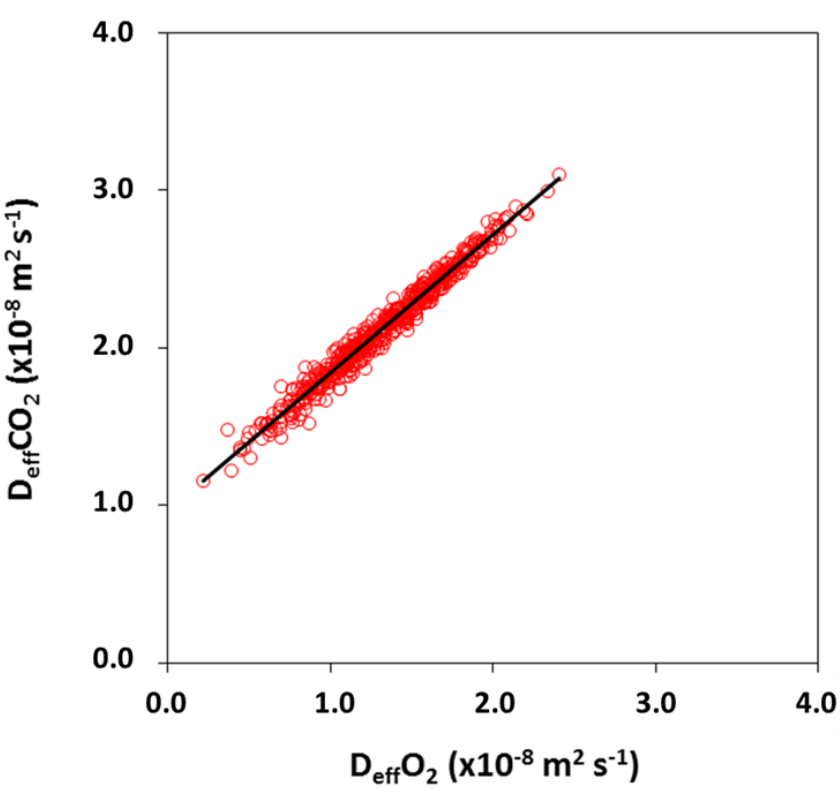

Figure 1. Linear correlation between effective O_2 diffusivity and effective CO_2 diffusivity computed by Ho et al. (2016).

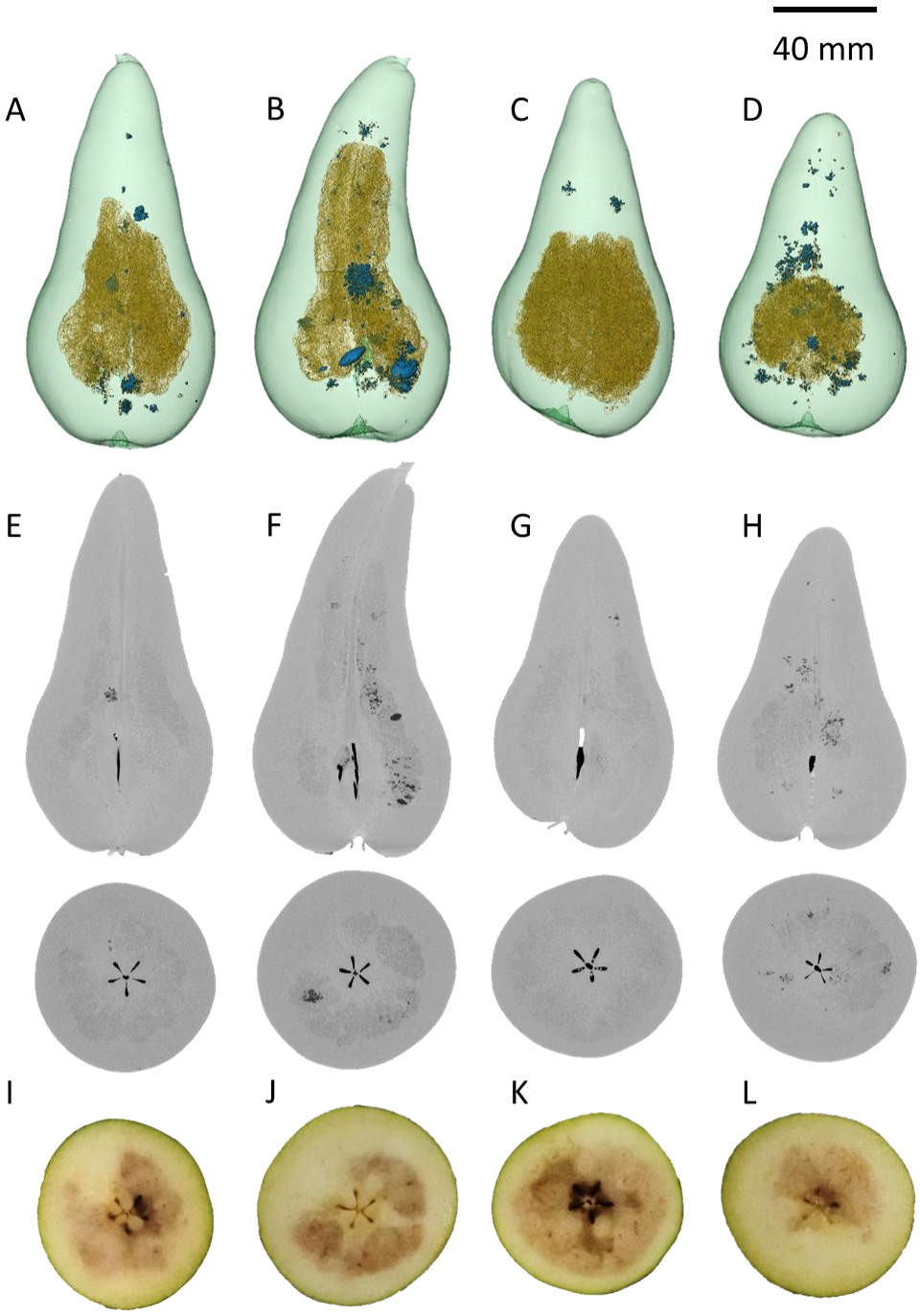

844

845 Figure 2. (A, B, C and D) 3-D geometry of affected pears (numbered 1 to 4) in which the brown
846 volume represents the browning symptoms and the small blue spots are the cavities. (E, F, G
847 and H) grayscale CT image of vertical (top) and horizontal (bottom) slices, (I, J, K and L)
848 photographs of corresponding horizontal pear slices.

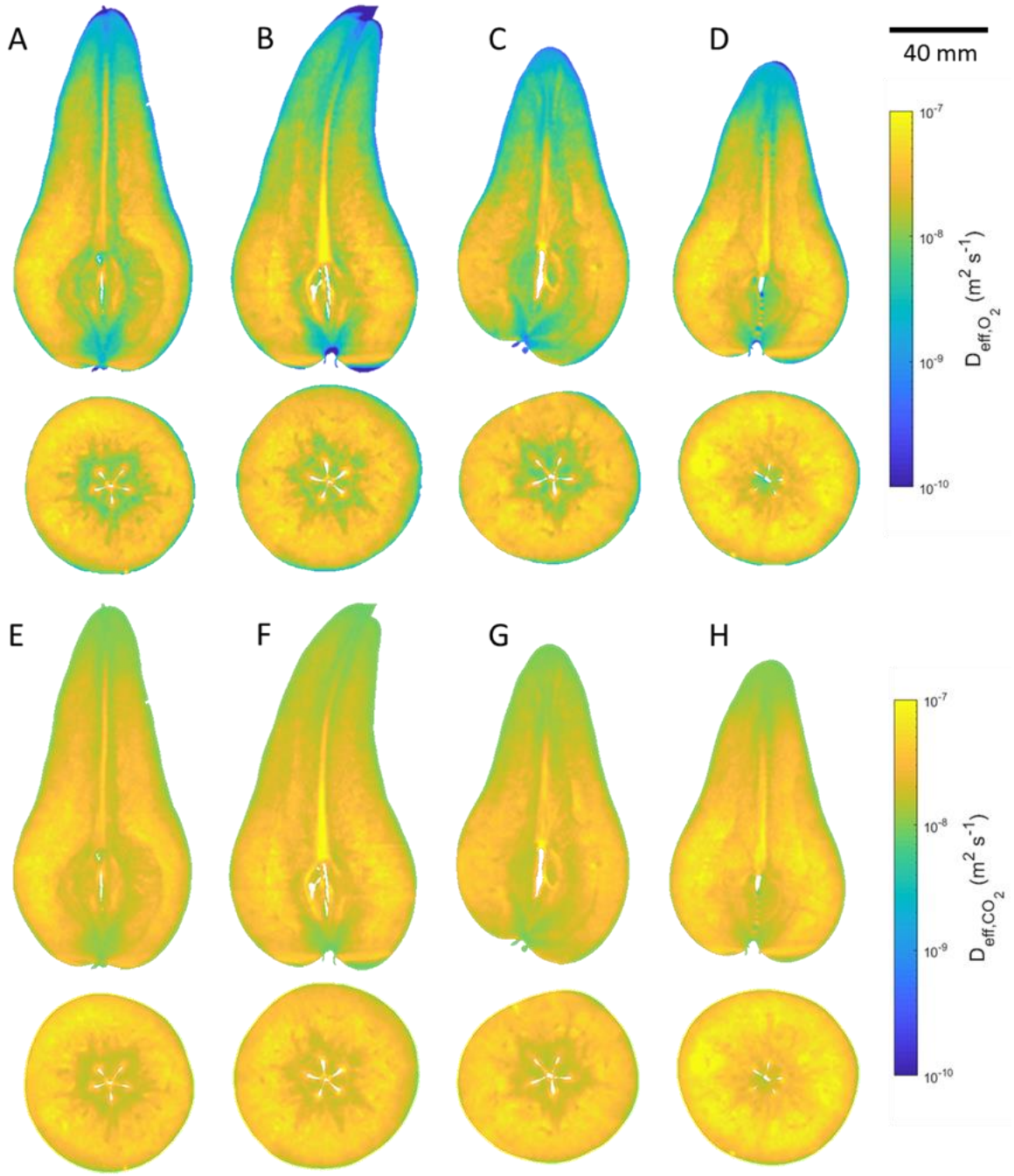

849

850 Figure 3. Effective diffusivity map of (A, B. C and D) oxygen and (E, F. G and H) carbon
851 dioxide of sound pears created using the developed models (Nugraha et al., 2021) and Equation
852 6, respectively.
853

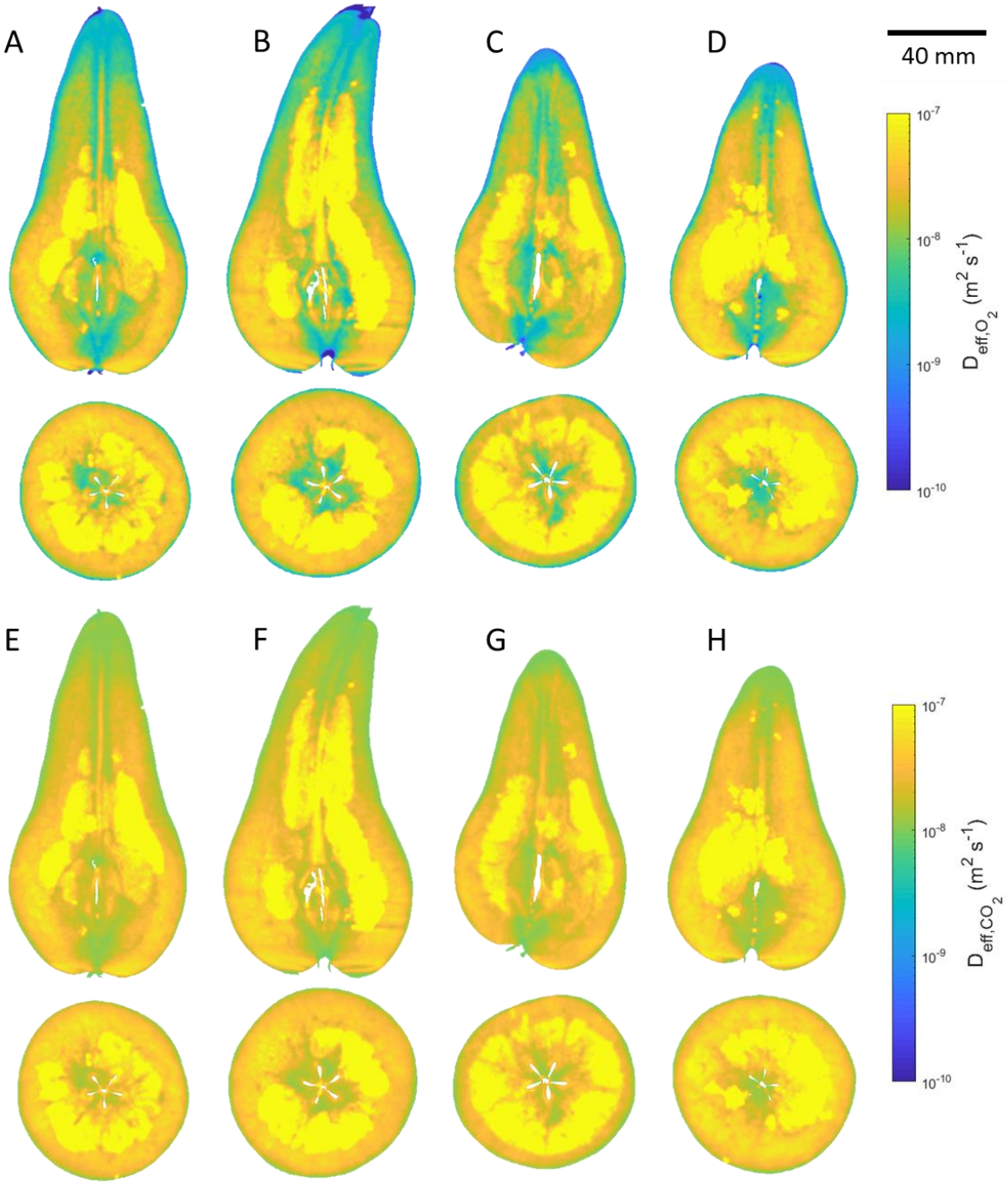

854

855 Figure 4. Effective diffusivity map of (A, B. C and D) oxygen and (E, F. G and H) carbon
856 dioxide of affected pears created using the developed models (Nugraha et al., 2021) and
857 Equation 6, respectively.

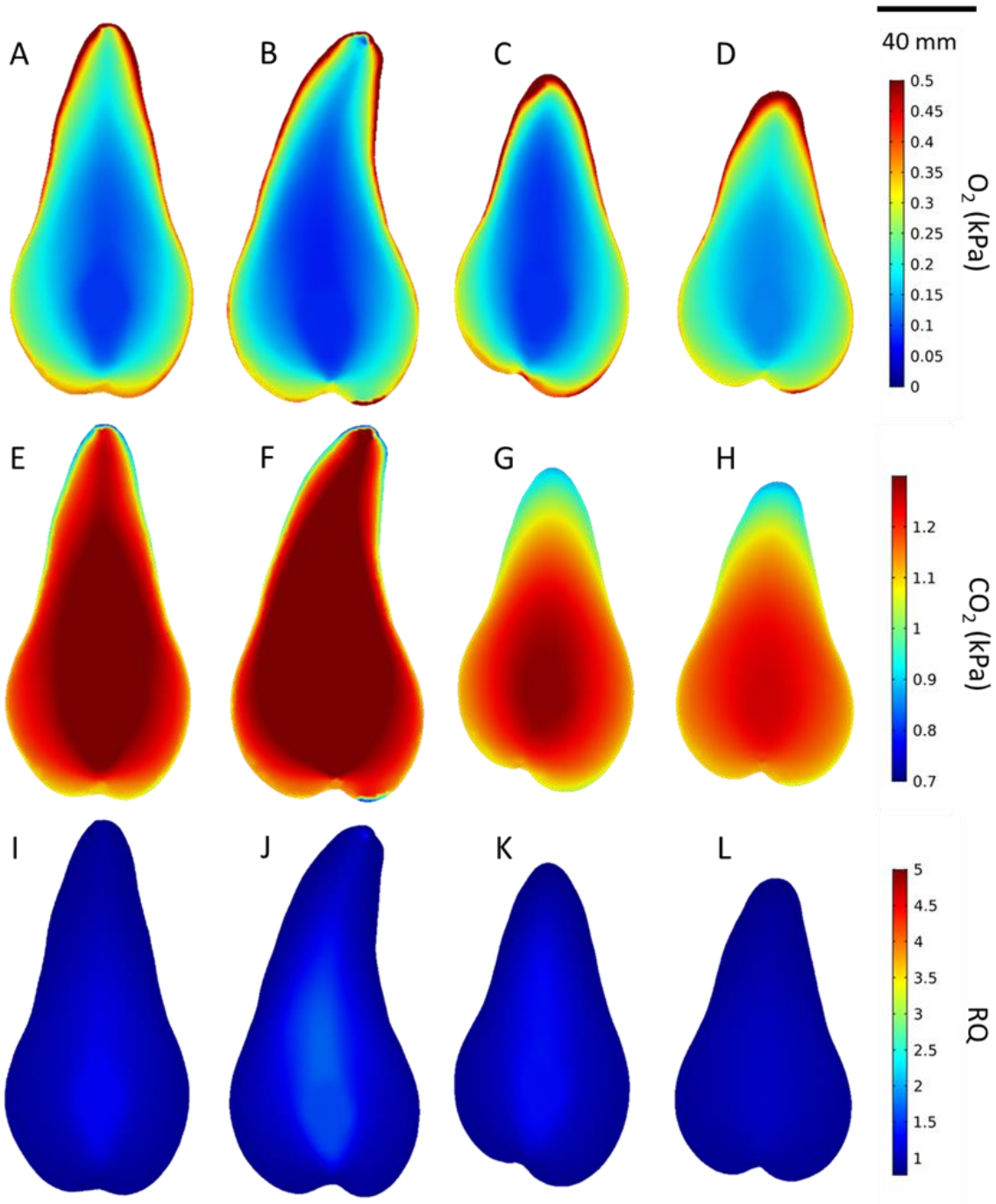

858

859 Figure 5. Internal O_2 (top) and CO_2 (middle) concentration, and RQ (bottom) profiles of (A, E,
860 I) pear 1, (B, F, J) pear 2, (C, G, K) pear 3 and (D, H, L) pear 4 predicted using the diffusivity
861 map at 1.0 kPa O_2, 0.7 kPa CO_2 and 1.0 ^{o}C.

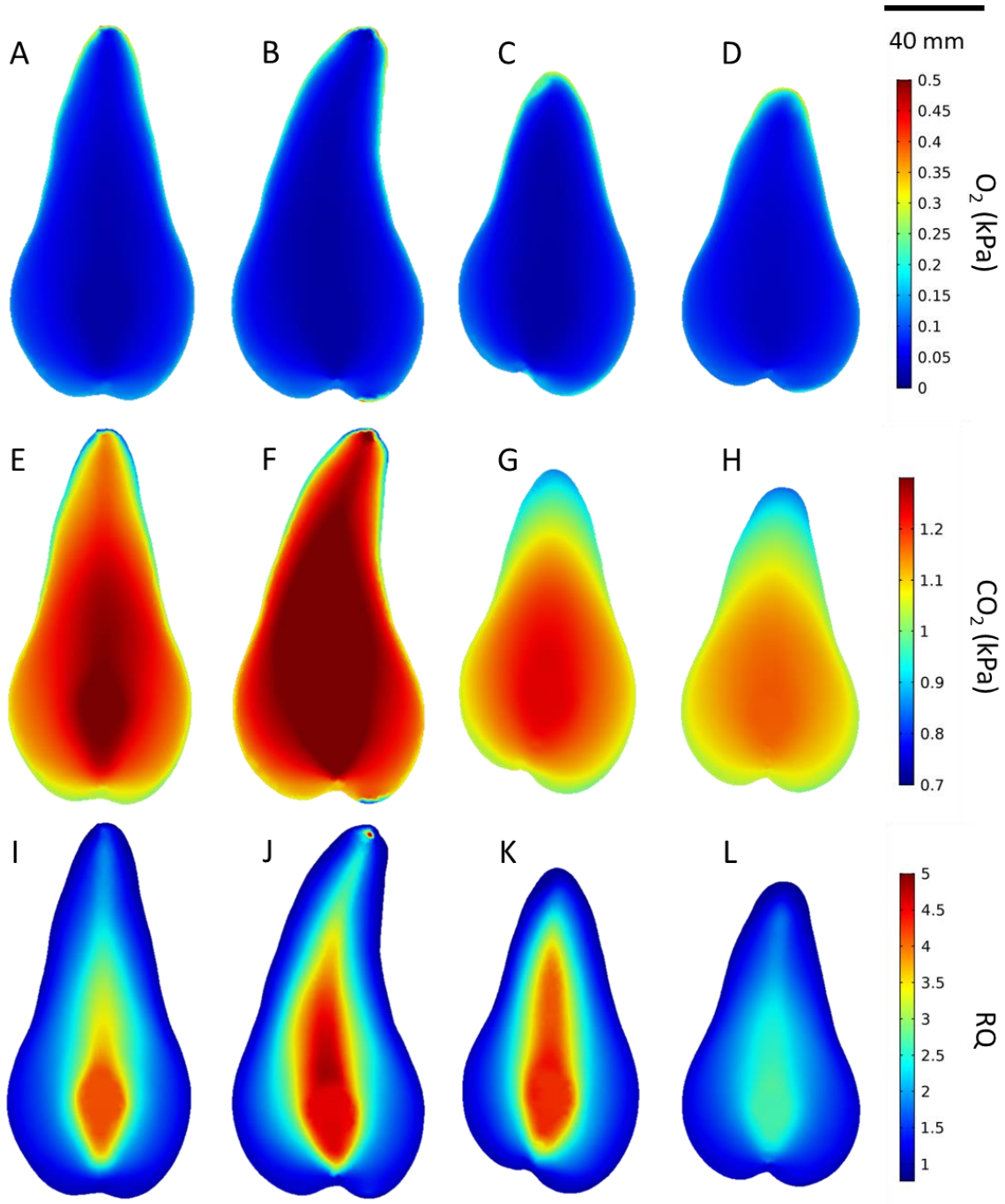

862

863 Figure 6. Internal O_2 (top) and CO_2 (middle) concentration, and RQ (bottom) profile of (A, E,
864 I) pear 1, (B, F, J) pear 2, (C, G, K) pear 3 and (D, H, L) pear 4 predicted using the diffusivity
865 map at 0.5 kPa O_2, 0.7 kPa CO_2 and 1 ^{o}C.

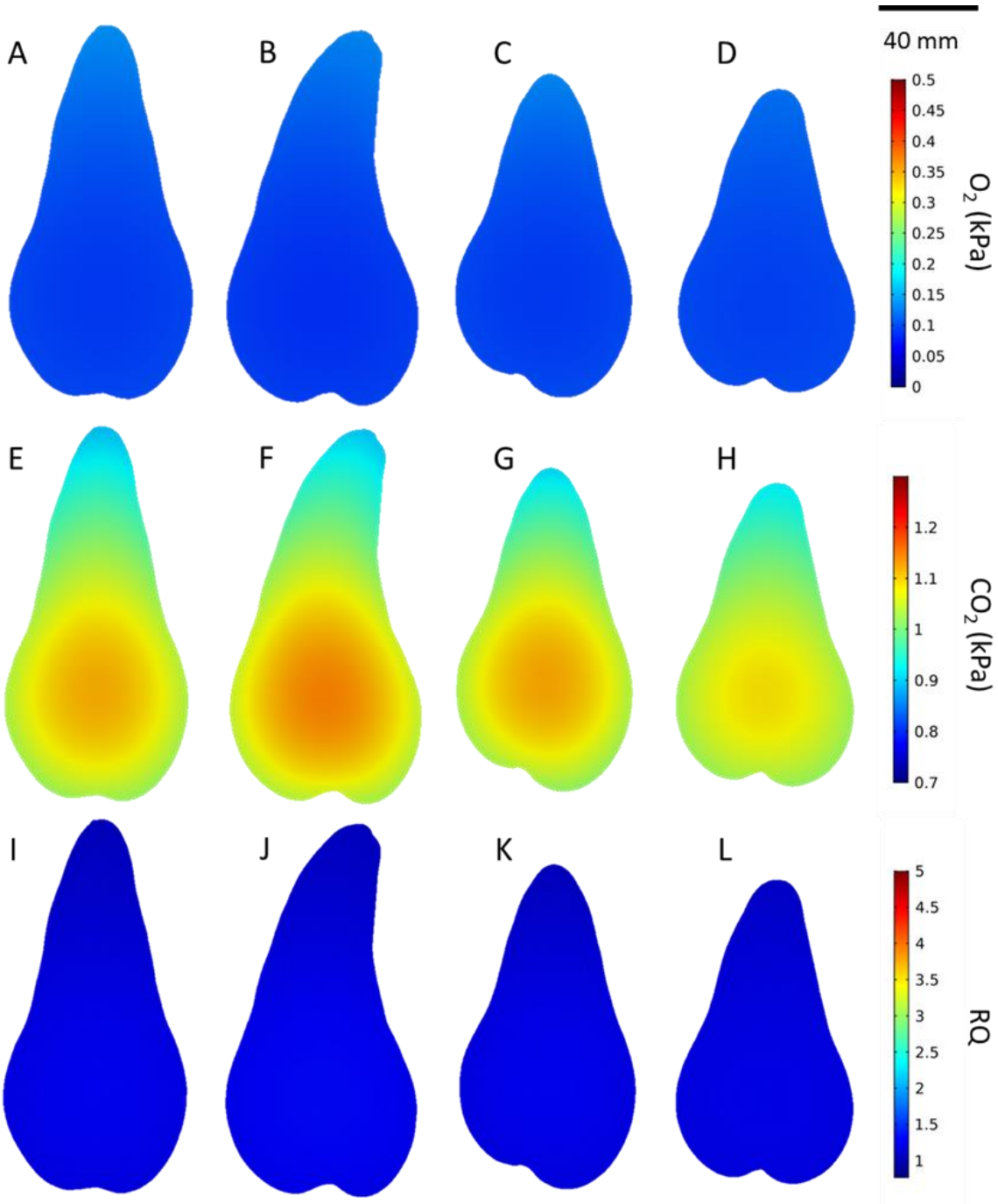

Figure 7. Internal O_2 (top) and CO_2 (middle) concentration and RQ (bottom) profile of (A, E, I) pear 1, (B, F, J) pear 2, (C, G, K) pear 3 and (D, H, L) pear 4 predicted using single diffusivity as the model parameter at 0.5 kPa O_2, 0.7 kPa CO_2 and 1 ^{o}C.

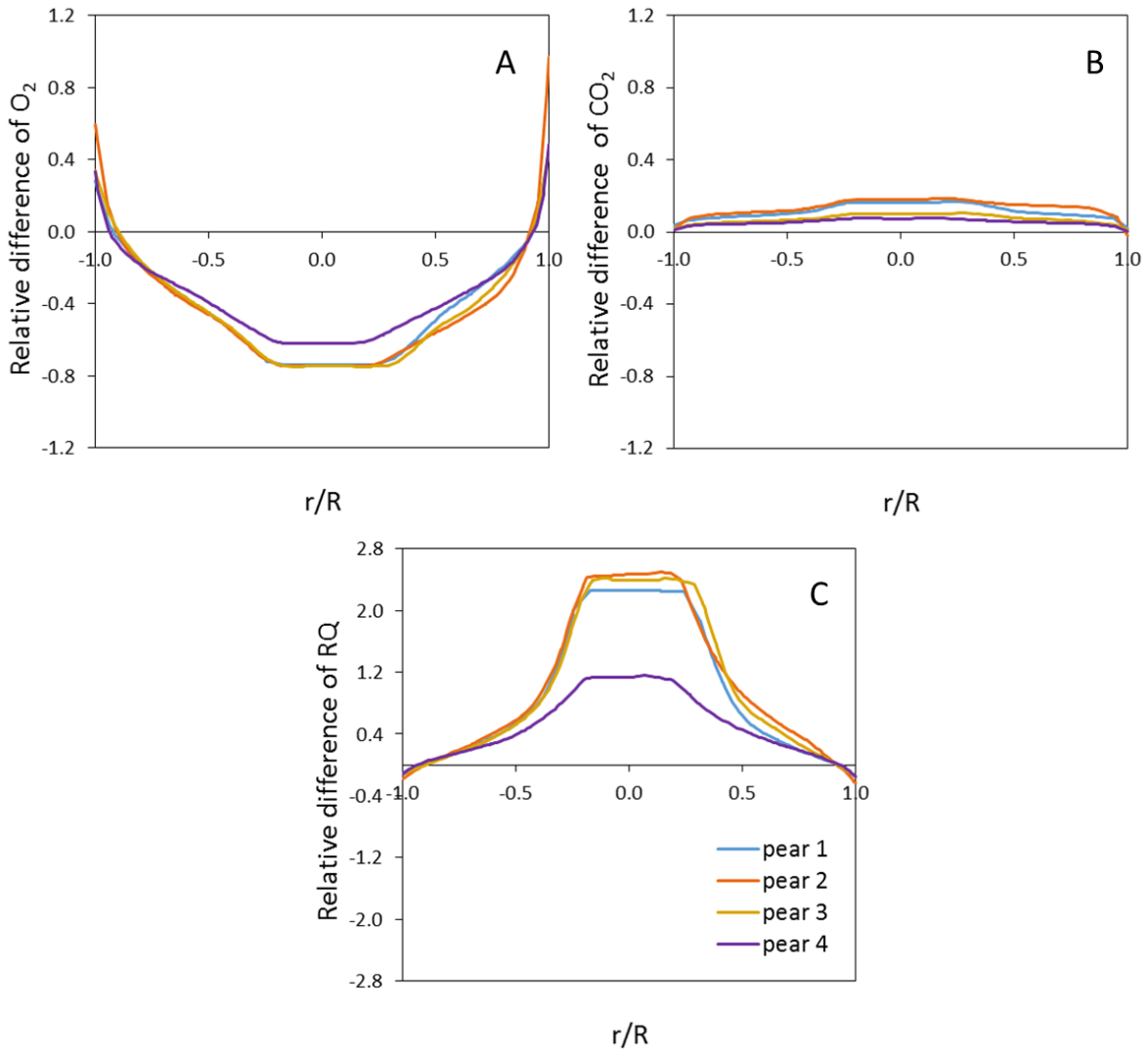

871

872 Figure 8. Relative difference profiles of (A) O_2 concentration (B) CO_2 concentration and (C)
873 RQ as predicted with the model incorporating the diffusivity map with respect to simulations
874 using a homogenous O_2 and CO_2 diffusivity at 0.5 kPa O_2, 0.7 kPa CO_2 and 1 ^oC. Values are
875 plotted as a function of the non-dimensional position along the radius (*r/R*) of the four pear
876 fruit samples.
877

878

879

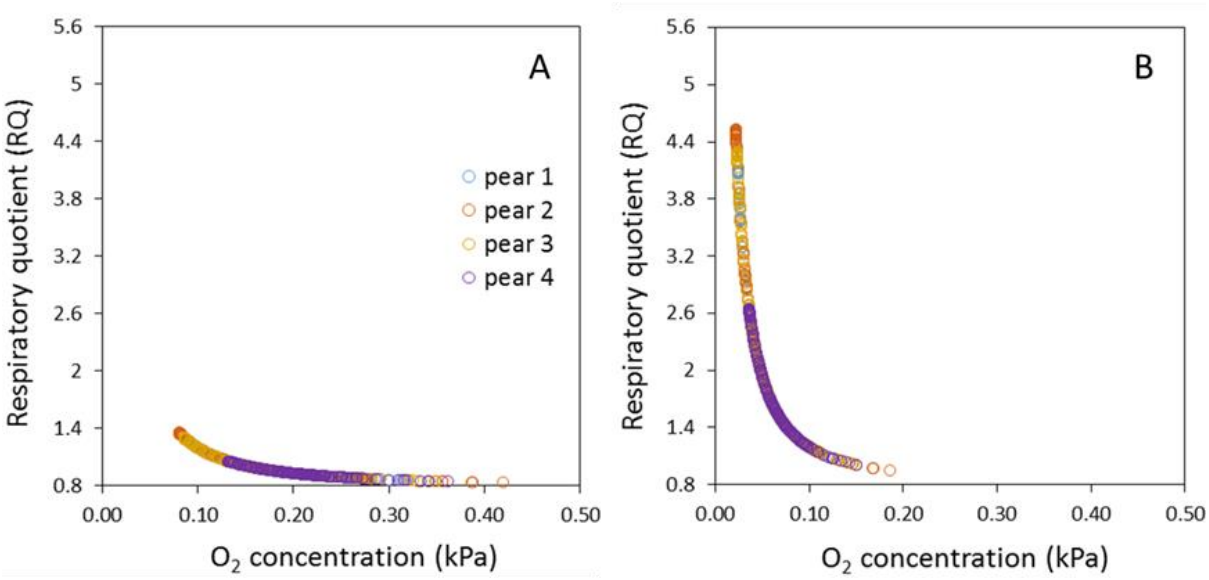

Figure 9. The change of the simulated RQ values as a function of the simulated O_2 levels in the pears at (A) 1.0 kPa O_2 and (B) 0.5 kPa O_2. Different colors represent different pear samples.

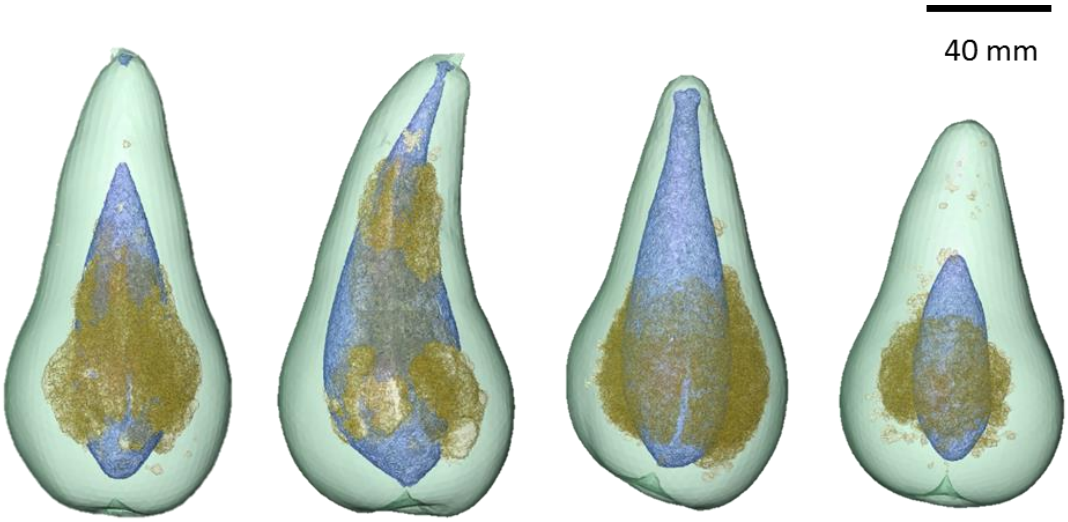

Figure 10. Browning area (brown color) imaged using X-ray CT and the area indicated to undergo fermentation (blue color) based on the predicted RQ values inside the pear. The fermentation process was indicated to be dominant when the *RQ** went above 2.12 (or at 0.044 kPa O_2).

Supplementary data

Supplementary 1

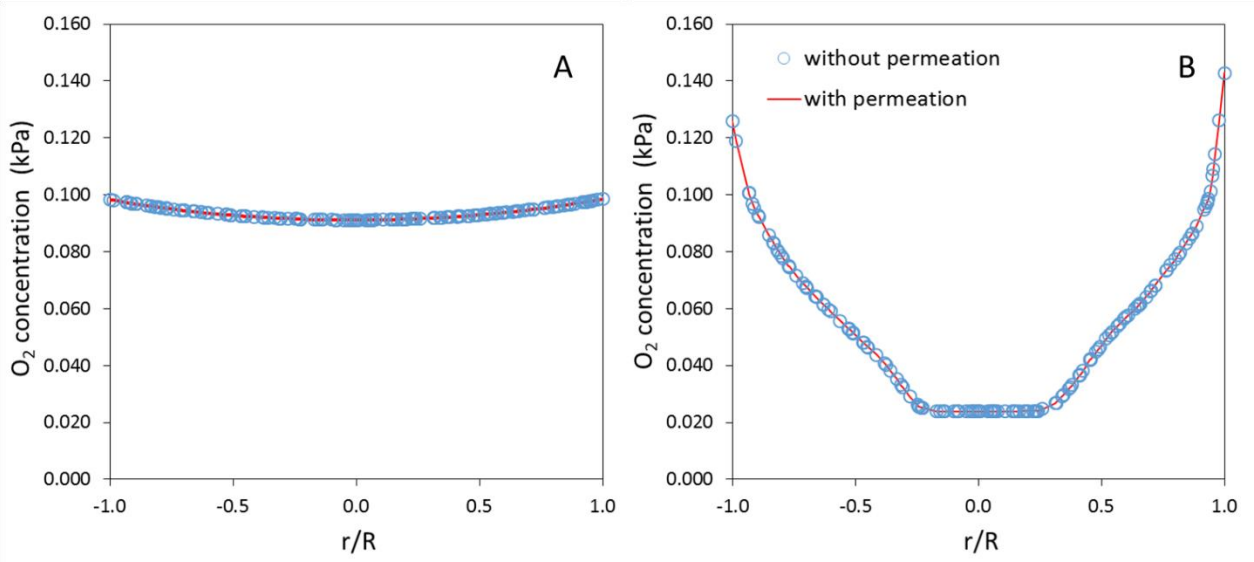

Figure S1. Effect of permeation on internal O_2 concentration along the equatorial axis of pear simulated using (A) single diffusivity and (B) diffusivity map at 0.5 kPa O_2, 0.7 kPa CO_2, 98.8 kPa N_2 at 1 °C. There is no obvious difference between the simulations. Values are plotted as a function of the non-dimensional position along the diameter (*r/R*) of the four pear fruit samples.

Supplementary 2

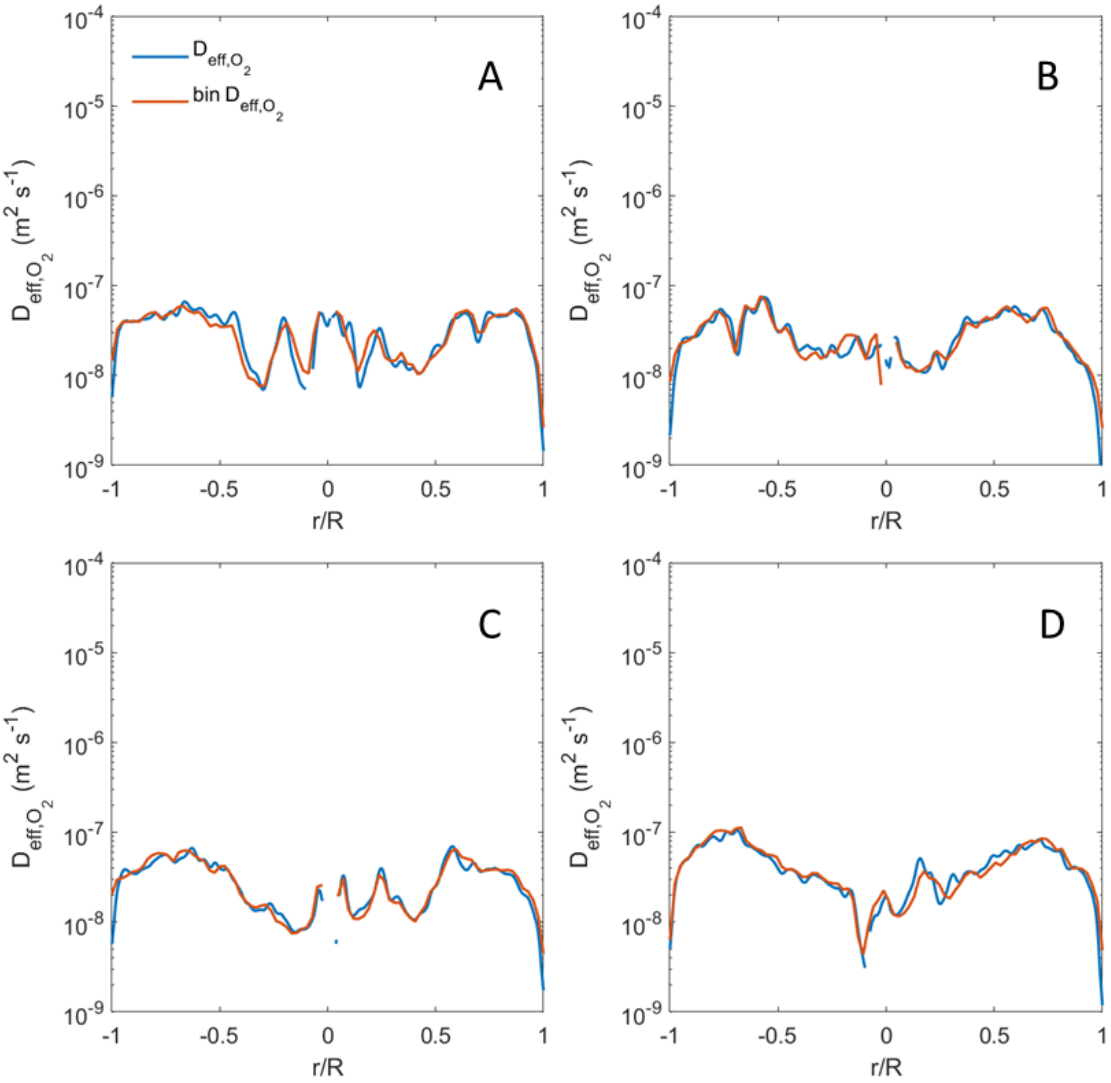

Figure S2. Profiles of effective O_2 diffusivity extracted from the diameter line of the original (blue line) and binned (red line) diffusivity maps of (A) pear 1, (B) pear 2, (C) pear 3 and (D) pear 4. The 10 voxels of the original maps were binned by means of an interpolation procedure in Matlab. Only small differences between the two profiles can be observed.

934 *Supplementary 3*

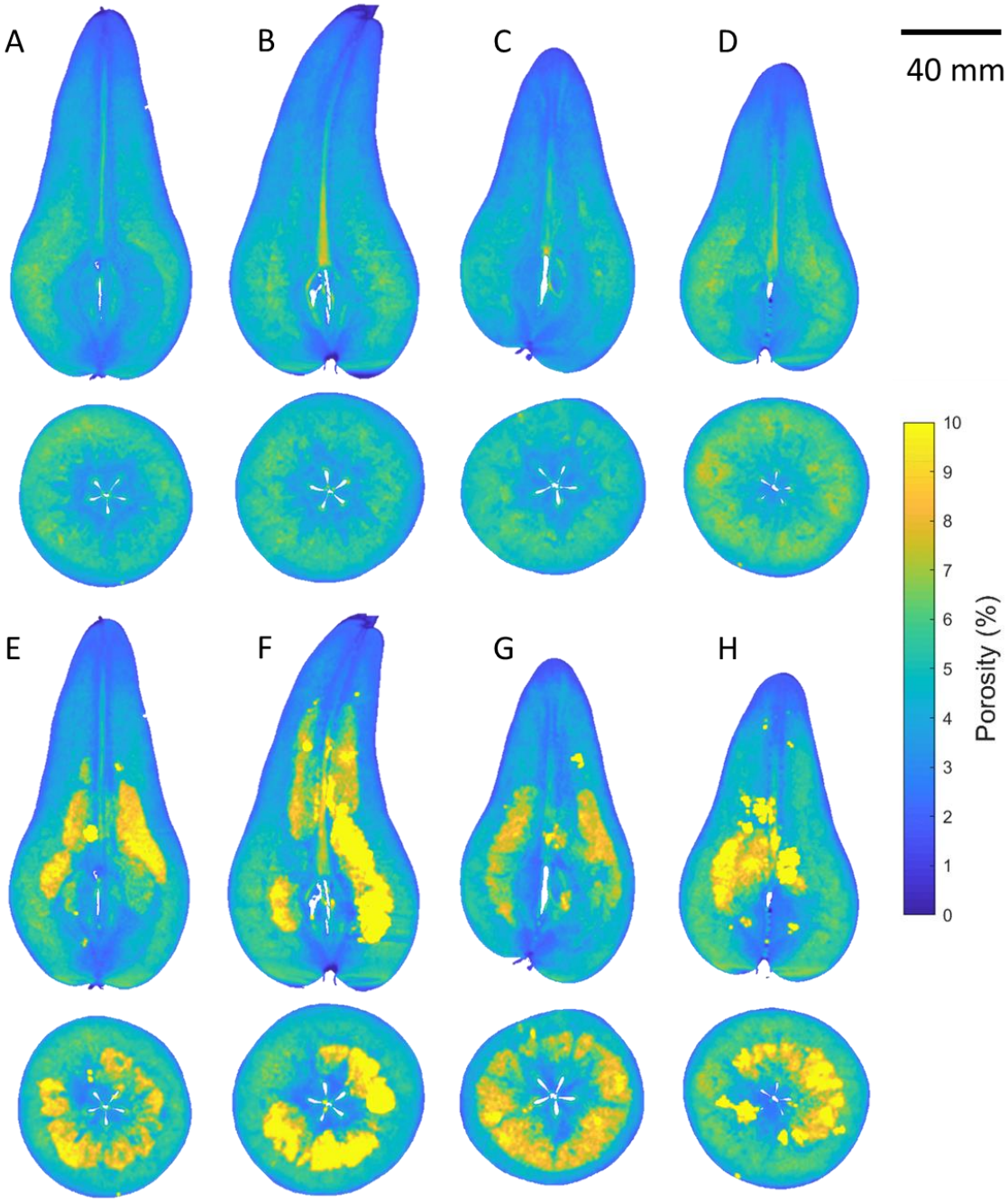

935

936 Figure S3. Porosity map of (A, B. C and D) sound and (E. F, G and H) affected pear created
937 using the developed models (Nugraha et al., 2019).
938

939

940

Supplementary 4

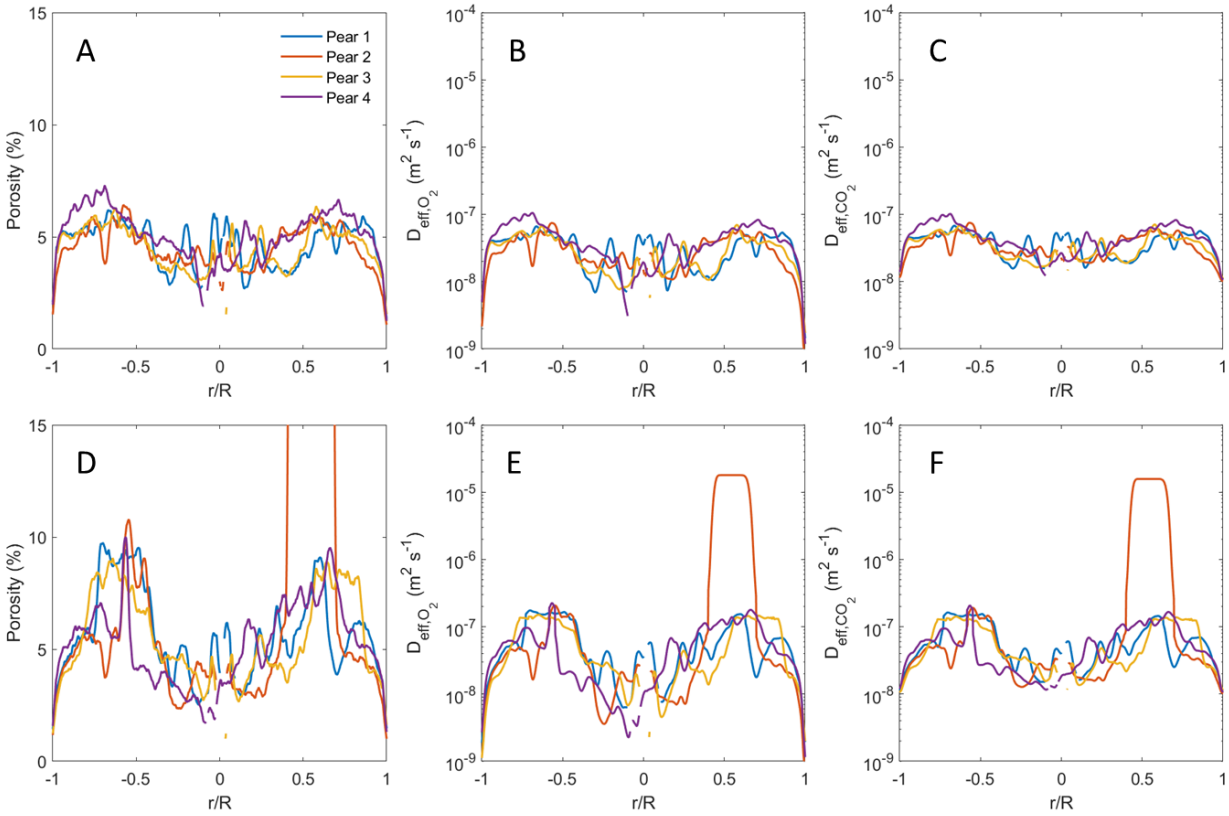

Figure S4. Profiles of (A and D) porosity, (B and E) effective O_2 diffusivity and (C and F) effective CO_2 diffusivity plotted as a function of the radius on the equator of the individual pears in (top line) healthy and (bottom line) browning-affected conditions. A profile that drastically increases at certain radius (*r/R*) is affected by a cavity.